ORIGINAL ARTICLE

Effects of physical modeling boundary conditions on the responses of 3 × 3 pile groups to liquefaction induced lateral spreading

S. Mohsen Haeri[1] · Morteza Rajabigol[1] · Saman Salaripour[1] · Ali Kavand[2] · Hiwa Sayyaf[1] · Sina Afzalsoltani[1] · Arian Asefzadeh[3]

Abstract

In this research, 1 g shake table experiments were conducted to evaluate the effects of boundary conditions on the responses of a 3 × 3 pile group to liquefaction-induced lateral spreading. For this purpose, a rigid and a laminar shear box with similar dimensions were designed and constructed at the Sharif University of Technology. The similitude laws for 1 g tests were implemented to construct the physical models. The profile of the soil layers consisted of a mildly sloped thick liquefiable layer between two non-liquefiable layers. The soil in the free field (far from the boundaries) and near or on the pile groups were fully instrumented to measure various parameters during and after shakings. The piles were also heavily instrumented with pair strain gauges to detect pure bending moments. The results, including acceleration and pore water pressure in various elevations of the free field, acceleration at the pile cap, surficial displacements, and bending moments in the piles, are presented and discussed in this paper. According to the results obtained from these two similar models (differing only by boundary conditions or containers), the response of the model implementing the rigid box is greater, possibly due to wave reflections from boundaries, limitation in movement, and bouncing back of the liquefied and spreading soil from the rigid walls.

Keywords 1 g shake table test · Liquefaction · Lateral spreading · Pile group · Boundary condition

✉ S. Mohsen Haeri
smhaeri@sharif.edu

1 Civil Engineering Department, Sharif University of Technology, Tehran, Iran

2 School of Civil Engineering, College of Engineering, University of Tehran, Tehran, Iran

3 Civil Engineering Department, University of Alberta, Edmonton, Canada

1 1. Introduction

Liquefaction-induced lateral spreading occurs in gently sloping grounds or grounds ending in a free face. This phenomenon is a common consequence of the liquefaction of a loose sandy layer at a shallow depth that is mostly overlain by a non-liquefied crust layer. In some cases, lateral movement of liquefied and crust layers may reach several meters and impose significant forces on the deep foundations of buildings and bridges. Severe damages to pile-supported structures due to lateral spreading have been observed in many strong earthquakes, e.g., Niigata 1964, Nihonkai-Chubu 1983, Hyogoken-Nambu 1995, Kocaeli 1999, Chi-Chi 1999, Bhuj 2001, Haiti 2010, Chile 2010, Tohoku 2011 earthquakes. Damaged piles in the aforementioned earthquakes indicate the importance of studying the effects of soil liquefaction and lateral spreading in the design of deep foundations (Imamura et al. 2004; Bhattacharya et al. 2013; Tamura 2014). In the last two decades, several studies have been performed to investigate various aspects of the response of piles to liquefaction induced lateral spreading using shake table tests (e.g., Ebeido et al. 2018, 2019a, b; Haeri et al. 2012, 2013, 2014; 2019, 2021; He et al. 2008, 2009, 2017; Kavand et al. 2012; 2014, 2021; Mao et al. 2019; Liu et al. 2017; Motamed et al. 2007; 2008; 2009; 2010; 2013; Motamed and Towhata 2010; Sato and Tabata 2011, Su et al. 2016, Suzuki et al. 2006; Tang et al. 2014; 2015), centrifuge tests (e.g., Abdoun et al. 2003; Imamura et al. 2004; Brandenberg 2005; Brandenberg et al. 2010; Dobry et al. 2003; Gonzalez et al. 2009; Knappett and Madabhushi 2012; Zhang et al. 2020), field blasting tests (e.g., Ashford et al. 2006; Juirnarongrit and Ashford 2006) and numerical methods (e.g., Chang et al. 2013; Li and Motamed 2017; Uzuoka et al. 2008; Wang and Zhang 2016). Numerous factors affect the response of deep foundations to lateral spreading, including boundary conditions, characteristics of input motion, thickness of the crust and liquefiable layers, numbers and arrangement of piles in a pile group, density of liquefiable layer, and so on. In this respect, a number of studies have been conducted to investigate the effects of some of the aforementioned parameters on the responses of piles to lateral spreading in the last two decades. For example, Imamura et al. (2004) conducted centrifuge model tests to investigate the effects of the number of piles and pile spacing in free head groups (2×1, 3×1 and 4×1 piles and spacing between 2 and 3D center to center) on the force applied to piles due to lateral spreading. It should be noticed that all piles of the groups were located in a single row. Imamura et al. (2004) found that the downstream pile of the groups experienced a lateral force of about 85% of that acting on the upstream pile. Imamura et al. (2004) also found that when the spacing between the piles was more than 4 times the diameter of the piles, there was no interaction between the piles. Uzuoka et al. (2008) employed a 3D finite element model to study the behavior of a 3×3 pile group behind a quay wall and found that the earth pressure on the piles from the crust layer was very important for the evaluation of the peak bending moment along the piles. The input motion in that study was applied perpendicular to the direction of ground flow. Motamed and Towhata (2010) and Motamed el at. (2010) carried out a series of shake table tests using a relatively small rigid box to investigate the effects of several parameters (e.g., soil density, characteristics and direction of input motion, and non-liquefiable crust layer) on the behavior of a 3×3 pile group behind a quay wall. Motamed and Towhata (2010) found that the amplitude, frequency, and direction of the input motion and also soil density had significant effects on the magnitude of lateral soil displacement. Moreover, the bending moment of the piles was drastically increased by the passive earth pressure due to the crust layer. He et al. (2008) and Haeri et al. (2012) studied and discussed the effects of the pile position of free head

groups (2×1 and 1×3) in sloping grounds without a non-liquefiable crust layer. They carried out shake table tests using relatively large rigid boxes. In both studies, the 2×1 pile groups were located in the ground slope direction, while in Haeri et al (2012) the 1×3 pile group was perpendicular to the ground slope direction. The input motions in He et al. (2008) and Haeri et al. (2012) were applied perpendicular and parallel to the ground slope, respectively. He et al. (2008) and Haeri et al. (2012) found that the downstream pile of the groups experienced a bending moment of about 40% and 90% of that in the upstream pile, respectively. Kavand et al. (2014) conducted shake table tests using a relatively large rigid box to study the behavior of the piles of 2×2 groups in a crusted liquefiable sloping ground. Kavand et al. (2014) found that various piles of the groups experienced different amounts of bending moments and lateral forces. Su et al. (2016) conducted a shake table test using a laminar shear box and studied the effects of lateral spreading on a pile in a single soil stratum behind a quay wall. Su et al. (2016) proposed a Beam on Nonlinear Winkler Foundation (BNWF) model to assess the influence of some parameters, e.g., elasticity modulus and diameter of the pile. Su et al. (2016) found that the pile head displacement decreased as the pile elasticity modulus increased, though the pile bending moment did not change. The results of Su et al. (2016) showed that pile head displacement and also bending moment increased as the pile diameter increased because a larger diameter can mobilize a greater soil wedge behind the pile. Liu et al. (2017) performed a shake table test using a laminar shear box on a 2×2 pile group in a single soil layer behind a quay wall and showed that the lateral pressure on the piles near the quay wall was about twice that of those far from the quay wall. Mao et al. (2019) carried out a series of shake table tests using a relatively small rigid box and studied the effects of lateral spreading on a 3×3 pile group in a single sloping soil stratum. Mao et al. (2019) found that the front (upslope) and the rear (downslope) piles carried much higher bending moments than those of the middle row piles. Haeri et al. (2014) and Kavand et al. (2021) carried out a shake table test using a relatively large rigid box. They investigated the behavior of piles of a dolphin-type berth in a sloping ground without a non-liquefiable crust layer and found that the piles position in the group was a key parameter and the downslope piles experienced higher bending moment than the upslope one.

Despite these valuable studies, there remains room for research on this subject as many aspects of the soil-pile interaction, especially in liquefied or laterally spreading conditions, are yet to be fully understood. One of the most important factors in the physical modeling of earthquake geotechnical problems is the boundary condition. Bhattacharya has summarized the soil boxes as follows: (i) rigid box; (ii) rigid box with flexible boundaries (e.g., sponge); (iii) rigid box with hinged end-walls; (iv) equivalent shear beam box; (v) laminar shear box; (vi) active boundary box. During shaking and propagation of S-waves through the soil layer, the soil next to the boundaries may undergo under compression and extension and P-waves may be generated. Thus, the response of the model will be affected by the interaction between P and S waves. Therefore, the reflection of the waves from the artificial boundaries must be taken into account. In an infinitely extended soil layer this phenomenon is absent since there are no boundaries and the energy of the waves diminishes with distance. In the most traditional box- the rigid box- the shear stiffness of the end walls is much higher than the stiffness of the layers of soil contained, while the design principle of a laminar shear box is to minimize the lateral stiffness of the container in order to ensure that the soil governs the response of the soil-box system. The main advantage of a laminar shear box compared to a rigid box is the reduction of the wave reflection and the P-wave generation (Bhattacharya et al. 2012). Kim et al. (2020) constructed a rigid box and a laminar shear box of similar size and carried out 1 g shaking table tests to investigate the effects

of boundary conditions on the results of a flat dry ground. Kim et al. (2020) compared the peak accelerations and response spectrum of the grounds and found that the soil accelerations at the center of the model and near the walls (boundaries) in the laminar shear box model were very close, in contrary to the rigid box model. In other words, the results of Kim et al. (2020) showed that a laminar shear box can better simulate the behavior of the infinite half space than a rigid box. Although the findings of Kim et al. (2020) research are valuable and fundamental, the results were obtained by comparing limited parameters (peak ground accelerations and response spectrum) of a wet compacted sandy soil in a level ground, in the absence of any foundations. However, the dynamic interaction of the piles and the liquefiable soils in sloping ground is a more challenging and complicated problem that is affected by numerous parameters.

In order to better understand the dynamic soil-pile interaction and specifically, the effect of boundary conditions on the response of the pile foundations to liquefaction induced lateral spreading, along the lines of the previous works, two physical models were constructed and tested at SUT shake table facilities to investigate the responses of two 3×3 pile groups to lateral spreading in two different containers (boxes), focusing on the effects of boundary conditions on the responses. In this regard, a large rigid box with a transparent side and a large laminar shear box were constructed and employed. The models consisted of a gently sloped non-liquefiable bottom layer overlain by a thick liquefiable layer and a surficial non-liquefiable crust. These layers were fully instrumented to measure different parameters, including accelerations and pore water pressures in the free field and adjacent to the piles, accelerations and displacements of the pile caps, and soil displacements at various points. In addition, the piles were instrumented with pair strain gauges to detect the pure bending moment in different sections of the piles. The results and analysis of these measurements are presented and discussed in this paper, although the test implementing rigid box has been briefly reported elsewhere (Haeri et al. 2013). It is worth mentioning that the ground profiles (the number of the soil layers, the density and the soil gradation of the layers, and the slope of the ground and the subsoil layers), pile groups geometry and material, physical modeling scale factors, and the input motions for both models were all identical. Therefore, the two experiments had identical characteristics except for their boundary conditions. Consequently, the reason for the differences between the results of these two experiments can only be attributed to the boundary conditions of these two models. Based on the authors' knowledge, this is the first time that the results of two different physical models of this size, with identical conditions except for the boundary conditions, have been studied, compared, and discussed.

2 2. Physical models

The models were constructed and tested using the shake table facilities at the Earthquake Engineering Research Center of the Sharif University of Technology. The shake table is a 4×4 m, 3 degrees of freedom facility capable of taking models of up to 300 kN. The rigid box was constructed with dimensions of 3.5 m length, 1 m width, and 1.5 m height. In order to monitor soil movement during lateral spreading, two large Plexi-glass windows were provided in one of the longitudinal sidewalls of the rigid box. The laminar shear box was designed and constructed for this research, with inner dimensions of 3.06 m length, 1.72 m width, and 1.8 m height, and outer dimensions of 4.2 m length, 2.4 m width, and 2.0 m height. Roll bearings were employed to minimize the friction between the 23 steel

laminates of the box. Figure 1 shows the rigid and laminar containers constructed and employed in this paper.

The Schematic plan and the cross-section of the models, including the layout of various transducers (acceleration, pore water pressure, displacement) are exhibited in Fig. 2. The main dissimilarity between the two experiments of this study is their containers or boxes (boundary condition). The other parameters e.g., the small change in the position of the pile groups within the boxes, a minor variation in the position of the sensors on the piles, and relatively small changes in the length and width of the boxes were not that effective on the obtained results of the study and could be neglected compared to the major change, i.e., the change in the boundary conditions or the type of the containers.

In this paper, the similitude laws proposed by Iai (1989) and Iai et al. (2005) were implemented. Considering the dimensions of the boxes (containers) in this study, a geometric scale of $\lambda_l = 8$ was selected. Based on the similitude laws, it was assumed that the scaled model and the prototype have the same density. However, for physical modeling tests conducted for the study of liquefaction and associated large ground deformations such as lateral spreading, Towhata (2008) suggested to employ very loose sand, which might be much looser than the in-situ sand so that the effect of reduced confining stress in the scaled model would be compensated by reduced density. As seen in Fig. 2, the soil profile in both models consisted of three primary layers: (1) a non-liquefiable base layer, (2) a thick liquefiable sand layer, and (3) a non-liquefiable crust layer. All layers were placed with a gentle slope of 4 degrees (7 percent). The base layer was constructed with very dense sand ($D_r = 80\%$) using the wet tamping method. Then, the container was almost filled with water. The liquefiable layer, with a relative density of about 15%, was constructed using the water sedimentation technique. In this method, a special bucket full of sand was moved with a constant velocity, and the sand was poured from almost zero height into the water to get the liquefiable layer as loose as possible. The crust (surficial) layer was constructed by dry deposition of a mixture of 88% sand and 12% clay with a liquid limit of 38% to produce clayey sand (SC) for casting a non-liquefiable crust layer. According to the guideline of the U.S. Army corps of engineers, soils with more than 10% fraction of finer than 0.005 mm, liquid limit (LL) greater than 36, and the ratio of water content to liquid limit less than 92%, are not susceptible to liquefaction (Finn et al. 1994; Kramer 1996). It should be noticed that the non-liquefiable crust layer was constructed by deposition of SC soil from the lowest possible elevation (almost zero height) to minimize the change in density of the underlying liquefiable layer. The sand used for the construction of all layers was standard Firuzkuh silica 161 sand, which is a uniform sand and is widely used in

(a) (b)

Fig. 1 Containers constructed and used in this study: **a** the rigid box, and **b** the laminar shear box
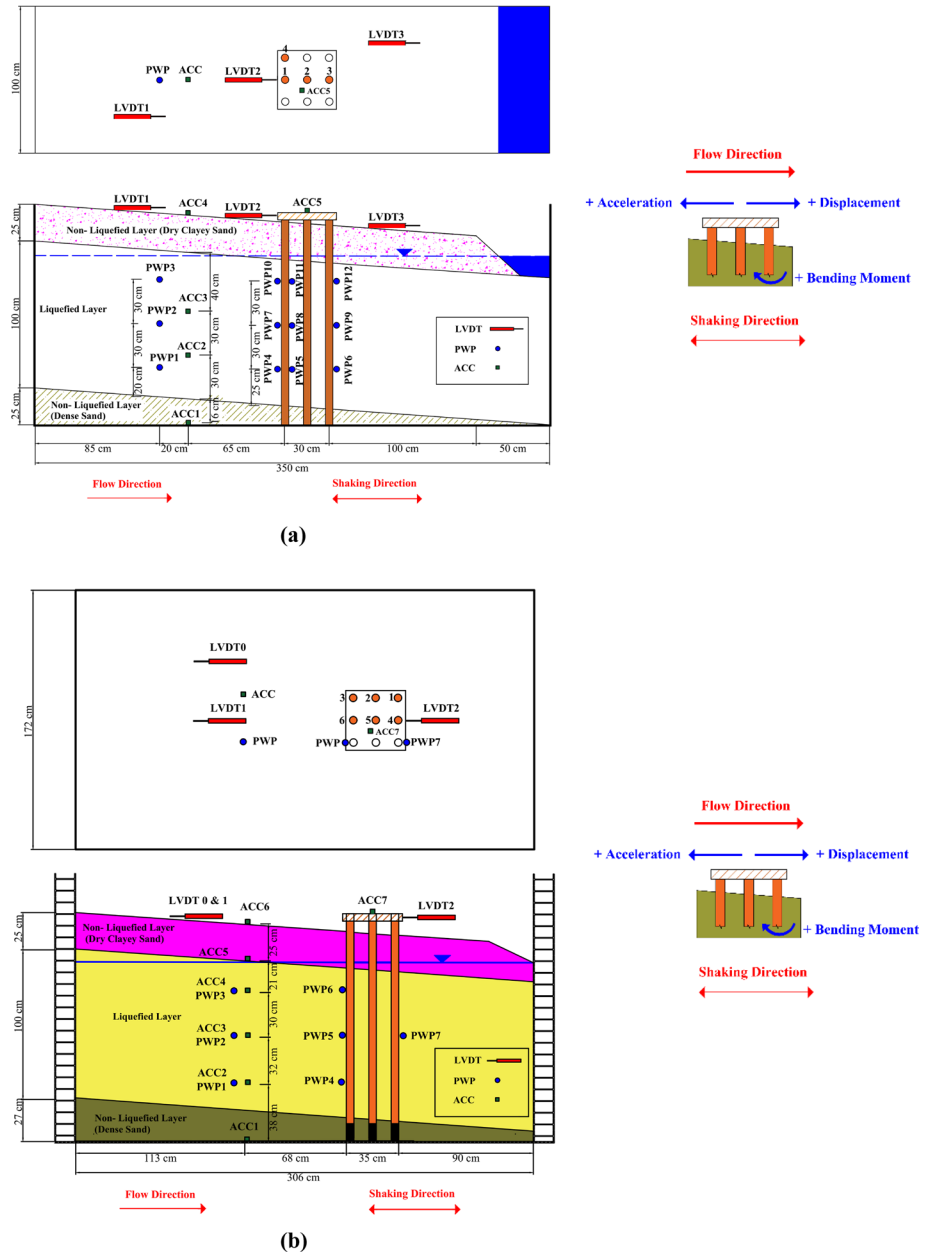
Fig. 2 Schematic plan, cross section of the physical models and diagram of the positive directions of different sensors: **a** the model with the rigid box, and **b** the model with the laminar shear box model

Iran for geotechnical testing. A summary of the properties and the gradation of the used sand is outlined in Table 1. When construction of the models was completed a grid was created over the ground surface, with gray color sand to detect lateral soil movement during and after the test. Then, an accelerometer was installed on the ground surface far from the boundaries

Table 1 Main properties of the Firuzkuh Silica Sand No. 161

Specific gravity	Mean grain size D_{50} (mm)	D_{10} (mm)	Maximum void ratio (e_{max})	Minimum void ratio (e_{min})	Coefficient of uniformity (C_u)
2.670	0.24	0.18	0.884	0.567	1.49

to measure surficial soil acceleration. Besides, in order to detect soil lateral movement, two LVDTs (Linear Variable Differential Transformer) were attached to a thin metal cup which was buried at shallow depths of the model. The cup (probe) was moving with the surficial soil during the shaking and associated lateral spreading and its movement was recorded by the data acquisition system.

For designing the model piles in this study, a prototype pile group was designed based on the Japan Road Association (JRA 2002) guideline to withstand the exerted lateral spreading forces considering the real geometry of the ground cross section. The geometrical and mechanical properties of the model piles were determined by using the aforementioned similitude laws.

The main properties of the piles are summarized in Table 3. All piles of the model were made of aluminum pipes (T6061 alloy). The center to center spacing of the piles was selected to be 3 times the piles diameter (D) which is a common practice for pile groups. The optimum spacing between the piles in a group is in the order of 2.5–3.5D (Bowles 1997) or 2.5–3.0D (Coduto 2001). Schematic views of the instrumented piles with strain gauges and the photo of the instrumented piles installed in the physical models are exhibited in Fig. 3. As seen in Fig. 3c, the strain gauges were covered with a multi-layer waterproof coating to protect them from wetting.

It should be mentioned that satisfying all the similarity laws in the model tests conducted under 1 g condition is not possible, thus the similarity laws that are involved in the main physical parameters of concern should be satisfied and the other relatively trivial ones can be neglected (Hamayoon et al. 2016; Zhu et al. 2021). In general, four independent dimensionless Buckingham π equations should be examined. According to the calculations presented in Table 3, the Buckingham π dimensionless similarity law π_1 is satisfied. However, similarity laws π_2, π_3, and π_4 are not satisfied. Based on the similarity laws proposed by Iai et al. (2005), the similarity ratios of the soil density (λ_ρ), the soil Young's modulus (λ_{Esoil}), and the soil hydraulic conductivity (λ_k) are assumed to be unity. In addition, as 1 g modeling test is conducted the gravitational acceleration similarity ratio (λ_g) is obviously equal to unity. Trying to satisfy the π_2 equation of Buckingham π theorem, the prototype pile can be considered to be a concrete pile with an elasticity modulus of 20 GPa and 40 cm diameter. However, considering Iai et al. (2005) similarity law for this study, the prototype pile can be a steel pipe with 40 cm outer diameter (Table 2). The similarity laws π_3 and π_4 do not approach the unity in 1 g physical model tests. The dissimilarity of the π_3 equation in Table 3, suggests that the rate of generation and dissipation of the excess pore water pressure in the model are different from those in the prototype. The dissipation rate of the excess pore water pressure in the model is higher than that in the prototype. The dissimilarity of the π_4 equation affects the pile displacement. In fact, the pile head displacement in the model would be different from that in the prototype. Since the main purpose of the present study has been the comparison of the behavior of two identical experiments, investigating only the effects of boundary conditions on the results of the tests, the scaling for both physical models are the same and therefore this issue of scaling might be of minor importance for this special study.

3 3. Test results and analysis

The results of the two identical physical models with different containers as discussed above are presented and analyzed to investigate the responses of the two 3×3 pile groups to lateral spreading, and also, to study the effects of boundary conditions on these responses.
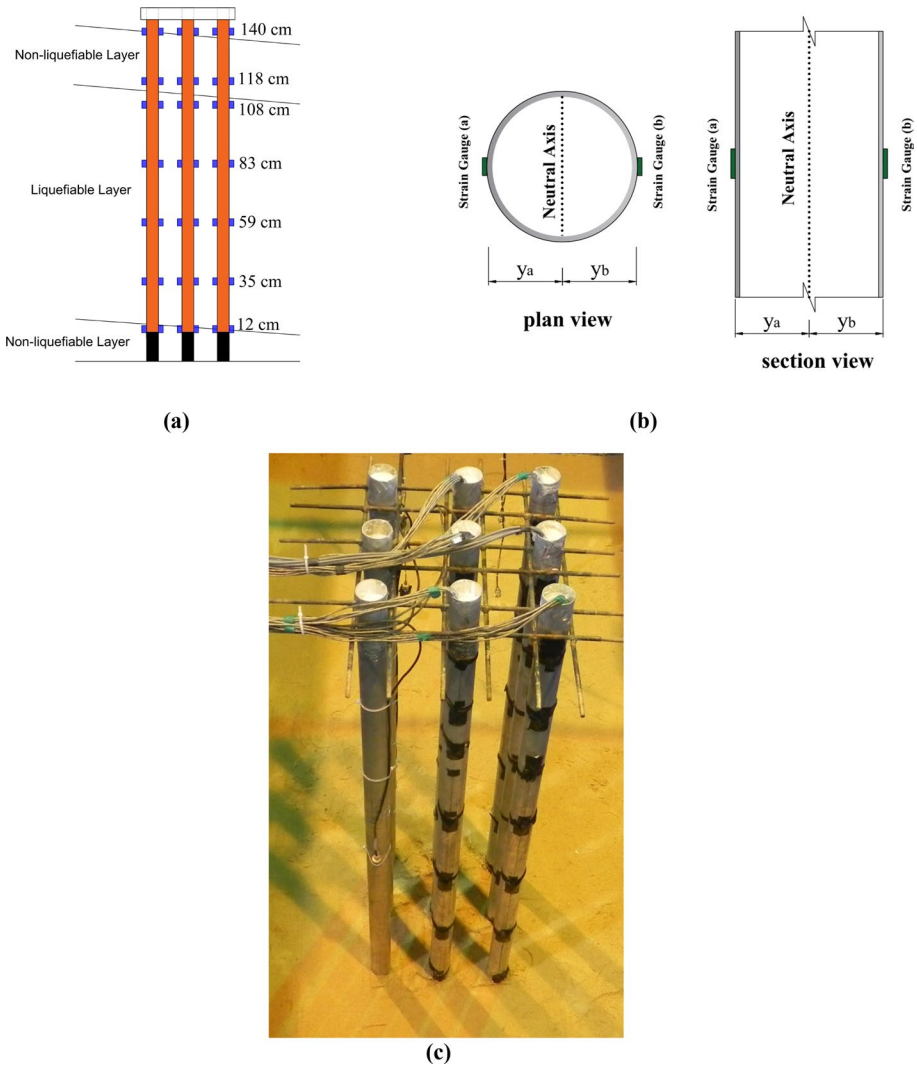
(a)

(b)

(c)

Fig. 3 Photos of instrumentation of the piles: **a** schematic view of an instrumented pile, **b** schematic plan and section of pair strain gauges on a pile, and **c** instrumented piles installed in the physical models

Table 2 Main properties of the piles in this study		
Parameter	Prototype	1 g Shake Table Tests
Material	Steel	Aluminum
Height (cm)	1200	150
Outer Diameter (cm)	40.0	5.0
Inner Diameter (cm)	37.6	4.7
Flexural Rigidity, EI (kN.m^2)	57,859	4.708

Table 3 Assessment of scaling factors in this study

Dimensionless π equations	π(prototype)/π(model)	Status of similarity [π(prototype)/π(model) = 1]
$\pi_1 = \frac{g}{L_{Pile}f^2}$	$\pi_1 = \frac{\lambda_g}{\lambda_{L_{Pile}}\lambda_f^2} = \frac{1}{8\times(0.35)^2} = 1$	Satisfied
$\pi_2 = \frac{EI_{Pile}}{E_{Soil}L_{Pile}^4}$	$\pi_2 = \frac{\lambda_{EI_{Pile}}}{\lambda_{E_{Soil}}\lambda_{L_{Pile}}^4} = \frac{12289}{1\times8^4} = 3 \neq 1$ (for steel pile, based on Iai's similitude law)	Almost not satisfied
	$\pi_2 = \frac{\lambda_{EI_{Pile}}}{\mu_{E_{Soil}}\mu_{L_{Pile}}^4} = \frac{5336}{1\times8^4} = 1.30$ (for concrete pile, based on Buckingham π)	Almost satisfied
$\pi_3 = \frac{k^2}{gL_{Pile}}$	$\pi_3 = \frac{\lambda_k^2}{\lambda_g\lambda_{L_{Pile}}} = \frac{1^2}{1\times8} = 0.125 \neq 1$	Not satisfied
$\pi_4 = \frac{\gamma_{soil}L_{Pile}}{E_{Soil}}$	$\pi_4 = \frac{\lambda_{\gamma_{soil}}\lambda_{L_{Pile}}}{\lambda_{E_{Soil}}} = \frac{1\times8}{1} = 8 \neq 1$	Not satisfied

Variables: length of pile (L_{pile}), frequency of loading (f), unit weight of soil (γ_{soil}), flexural rigidity of pile (EI_{Pile}), Young's modulus of soil (E_{Soil}), hydraulic conductivity of soil (k), gravitational acceleration (g)

The test results include accelerations, displacements, bending moments, pore water pressures, and p-y curves.

3.1 Accelerations in the free field

According to Fig. 2, accelerometers were installed at various elevations of the models and an adequate distance from the piles and the boundaries. Time histories of soil acceleration in the free field of the models were compared in Fig. 4a. Identical input motions, including 30 sinusoidal cycles with an amplitude of 0.3 g and a frequency of 3 Hz having two 3 cycles ascending and descending ramps, were applied to the models. The applied base shaking motion was parallel to the ground slope in both experiments. Despite the identical shaking input, different acceleration responses at various points of the ground were obtained. Comparing time histories of the acceleration at the ground surface of these two models illustrates that the acceleration at the ground surface of the model with the laminar shear box attenuated after liquefaction, but the surface acceleration for the model with the rigid box behaved differently, even after triggering of liquefaction. Large spikes with a positive sign in acceleration exhibited greater surface acceleration in the upslope direction in the model with the rigid box. This could be due to the reciprocal reactions of the bouncing back of the pile group and the downward movement of the soil mass due to lateral spreading. It seems that the wave reflections from the rigid walls caused an amplification of acceleration at the surface layer. Likewise, the soil acceleration at the middle of the liquefiable layer in the model with the rigid box is greater than that in the other model. The amplitudes of accelerations at the surface and the middle of the liquefiable layer in the rigid box model were respectively, 87% and 198% more than those obtained using the laminar shear box model. This issue can be attributed to the effects of boundary conditions. The maximum values of soil acceleration at different elevations of the free fields in both models are compared in Fig. 4b. According to this figure, the maximum acceleration at the ground surface was greater than that at the middle of the liquefiable layer in both models. Amplification occurred due to wave propagation in the non-liquefiable crust layer. As seen in Fig. 4b, the
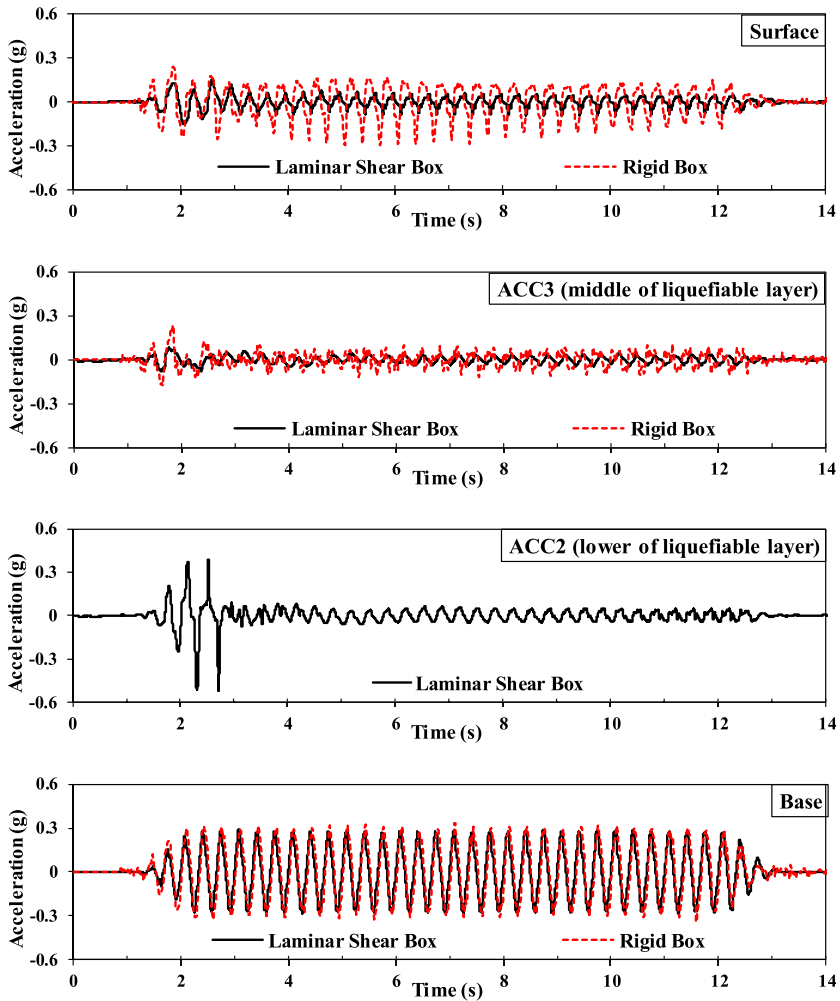
(a)
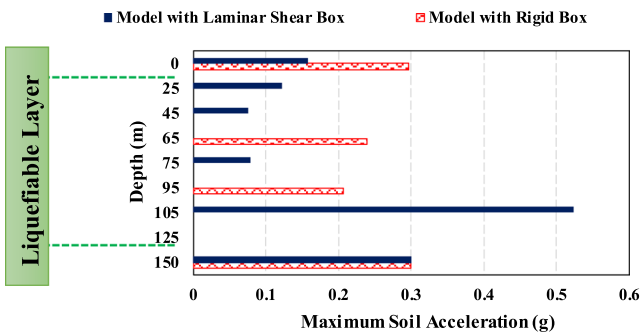
(b)

Fig. 4 The results of free field acceleration: **a** time histories of accelerations at different elevations of the models, and **b** the amplitudes of soil acceleration at different elevations of the models

amplitudes of acceleration at the free field were greater in the model with a rigid box compared to those in the laminar shear box due to boundary condition effects.

An accelerometer, ACC2, was placed at a lower depth of the laminar shear box model, see Fig. 2b. The results indicate that an amplification should have occurred in the acceleration at this elevation, due to wave propagation in the underlying non-liquefiable layer. The amplified acceleration was approximately 80% greater than the amplitude of the input motion and occurred at the starting cycles of the loading, before liquefaction. After liquefaction, the amplitude of the acceleration at the lower depth of the liquefied layer dropped to the very low amount of 0.07 g, an 87% drop in the amplitude of acceleration for ACC2 meaning that by the continuation of shaking the lower parts of the liquefiable soil also started to liquefy and consequently a huge drop in acceleration occurred. It should be noticed that ACC2—the accelerometer in the lower depth of the liquefiable layer- in the rigid box model was recording soil acceleration properly before liquefaction triggering, but after liquefaction started, no data was recorded, which might be due to disconnection of its wire. Hence, the authors did not show the time history of this accelerometer in Fig. 3a to prevent imprecise interpretation.

3.2 Comparison of the built up excess pore water pressure in two models

Several transducers were employed to measure excess pore water pressure in the free field and near the pile groups in both models. Time histories of r_u (ratio of excess pore water pressure to initial effective stress) at different locations in the free field and near the piles of the models are shown in Fig. 5. As seen in this figure, liquefaction was simultaneously triggered in both models at 2.5 s (3rd cycle of the main shaking). The results showed a higher rate of dissipation of excess pore water pressure near the piles in the model with the rigid box. It can be attributed to the effects of the larger gap occurred between the piles and the soil in the model with the rigid box comparing it with that of the model with the laminar shear box (Fig. 6). The larger gaps between the soil and the piles in the case with rigid box were possibly due to the effects of the boundary condition and higher energy trap in the rigid box. In other words, the relative displacements between the piles and the laterally moved soil were larger in the rigid box model. As seen in Fig. 6, the generated gaps between the piles and the crust in the rigid box model were larger than those in the laminar shear box model. Also in Fig. 6, heave at the upslope of the pile groups can be seen which should be taken into account when designing piles against lateral spreading. Heave at the upslope of a single pile was observed reported and discussed by Haeri et al. (2012).

3.3 Displacements of the soil and the pile cap

Two LVDTs (LVDT1 and LVDT2) were placed at similar positions on the ground surface of the models to measure the free field displacements. In order to detect soil lateral movement, the LVDTs were attached to thin metal cups which were buried at shallow depths from the model surface. The cups (probes) were moving with the surficial soil during the shaking and associated liquefaction and lateral spreading. It should be noticed that the ground settlement affects the location of the probes and the measurement of the soil deformation during the test. Several professional cameras were employed to record the models from various viewpoints before, during, and after the shaking. The ground settlement and then the angles between LVDTs and the probe were determined by processing images recorded by side cameras. Then the data measured by
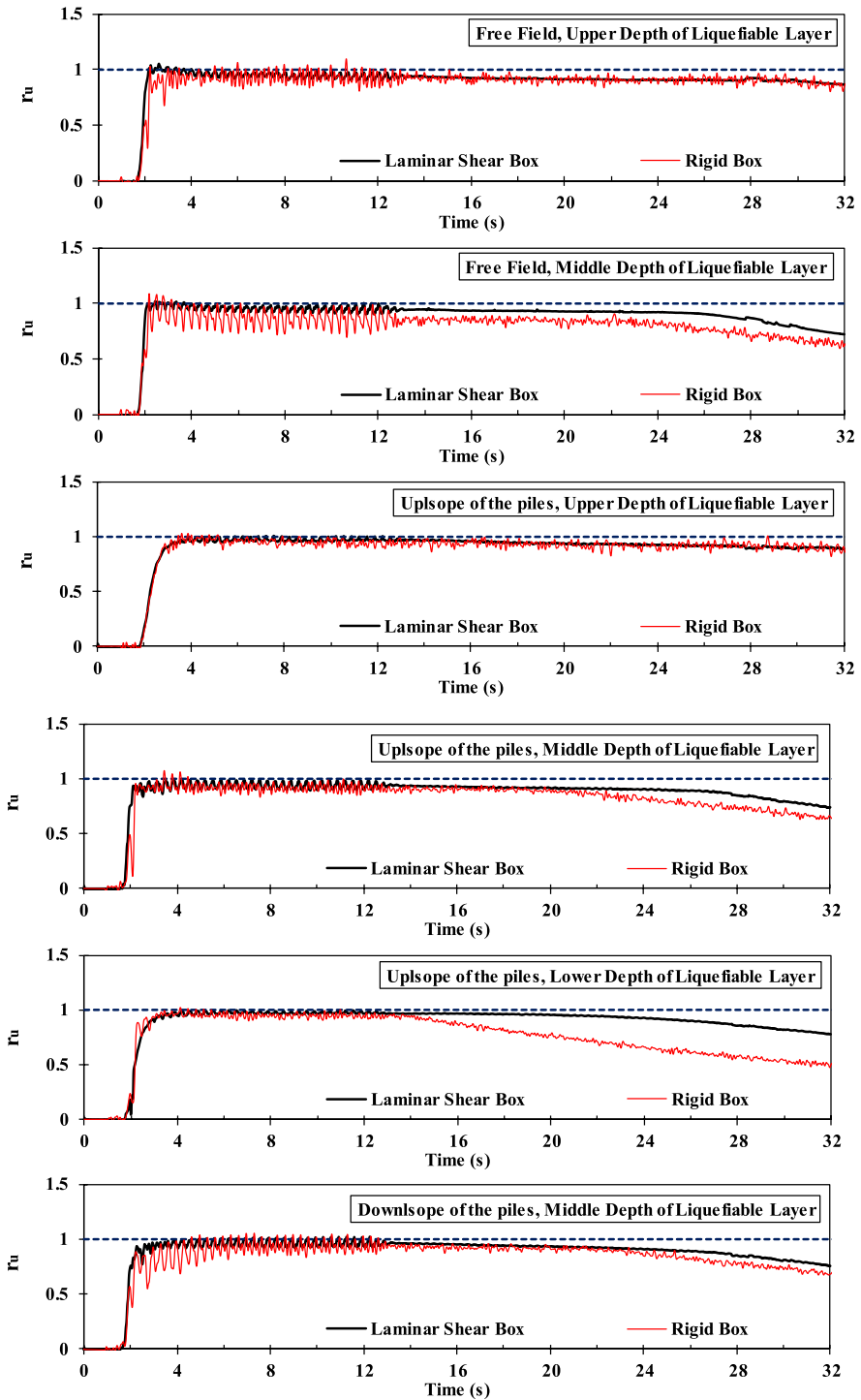
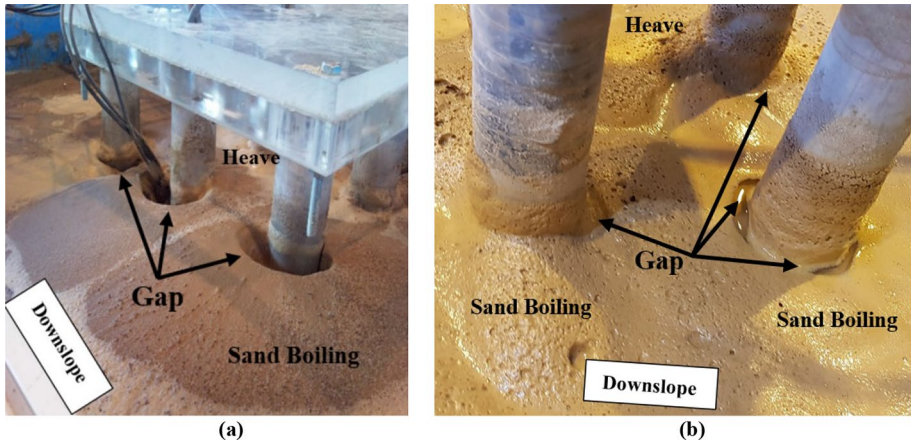**Fig. 5** Time histories of r_u value in both models

Fig. 6 The gaps between the soil and the piles: **a** in the rigid box model, **b** in the laminar shear box model

LVDTs were modified to represent the pure lateral soil displacements. Time histories of the free field displacements based on measurements of LVDT1 are shown in Fig. 7a. The positive sign in this figure shows the downslope lateral movement of the soil. In the model with a rigid box, the maximum and final (residual) free field soil displacements in the rigid model were approximately 20% and 40% greater than the other model, respectively. It seems that a higher level of energy reflected from the walls of the rigid box model has been responsible for the higher response compared to that of the laminar box.
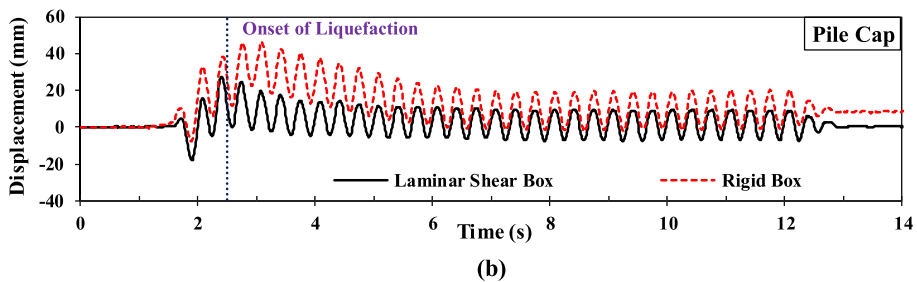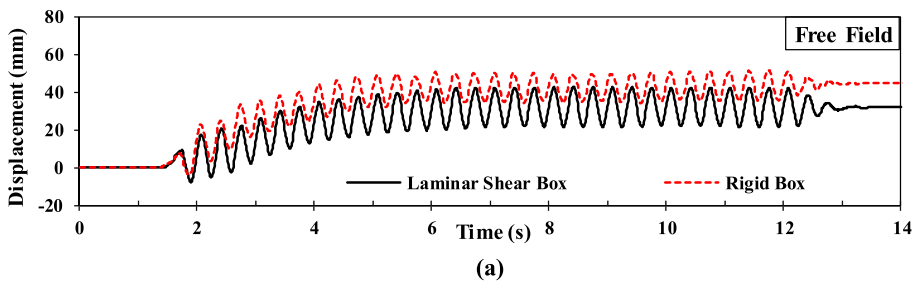
Fig. 7 Time histories of displacement in the models: **a** free field, and **b** pile cap

In each model, one LVDT was also attached to the pile cap. Time histories of the displacement of the pile caps for the two models are compared in Fig. 7b. A positive sign in this figure shows pile cap downslope movement. Based on the excess pore water pressure measurements (Sect. 3.2 of this paper), liquefaction occurred almost simultaneously in both models at an approximate time of 2.5 s. At that specific time, r_u (the ratio of the excess pore water pressure to the initial effective stress) reached the unity at the free field of both models (Fig. 5). It is notable from Fig. 7b that the maximum displacement of the pile cap for both models occurred approximately at the onset of liquefaction triggering. Afterwards, the pile groups bounced back in both models due both to the stiffness of the pile group and the loss of the shear strength in the liquefiable layer. The pile cap displacement in the rigid box model was more than that in the laminar shear box model, similar to the free field displacement. The maximum displacement of the pile cap in the model with the rigid box is about 70% more than that for the model with the laminar shear box. The pile group in the laminar shear box model fully bounced back to its initial position; however, the residual displacement in the pile group of the rigid box model was approximately 8 mm.

3.4 Bending moment induced in the piles

The piles in both models were fully instrumented with pairs of strain gauges to measure pure bending moments. Note that the piles were installed in steel tubes (with a height of 10 cm) which were welded to the base of the boxes. Hence the piles were fixed at the bottom in translational and rotational directions in order to model a long pile fixed at the bottom in a non-liquefiable soil layer. The pile heads were pushed in the prepared holes of the cap made of plexiglass which did not provide a complete rotational fixity for the piles. Thus, the provided fixity of the piles inside the pile cap of the pile group was not significant and clearly known. Amounts of bending moments at different sections of the piles were determined by the Euler–Bernoulli beam theory. The maximum bending moment for all the piles occurred at the lowest section (i.e., the boundary between the liquefiable layer and the underlying non-liquefiable layer or the fixity point, depth = 138 cm according to Fig. 3a). In this paper, the responses of the corresponding piles in the models are compared to investigate the effects of boundary conditions on them. The responses of the 3×3 piles to lateral spreading for each model are presented and discussed as well, to study the effects of pile position in the groups.

3.4.1 3.4.1. The effects of boundary conditions on the response of the piles

Figure 8 compares the time histories of the bending moments at the lowest sections of the corresponding piles in the models. The positive sign in Fig. 8 shows the upslope concave deflection of the piles (see Fig. 2). In both models, bending moments approached the maximum value almost simultaneously on liquefaction triggering at the time of about 2.5 s. According to Fig. 8, just after the liquefaction, bending moments in the piles of both models started to decrease gradually during shaking, because of the reduction in the liquefied soil strength around the piles and bouncing back of the piles due to elastic rebound as discussed before. As seen in Fig. 8, the piles in the rigid box model showed a greater response to the loading. In order to better evaluate the effects of boundary conditions on the behavior of the piles subjected to liquefaction induced lateral spreading, bar charts of the relative maximum bending moments ($M_{max, \text{model with rigid box}}$/ $M_{max, \text{model with laminar shear box}}$) are given in Fig. 9. The maximum bending moment experienced by piles in the model with the rigid
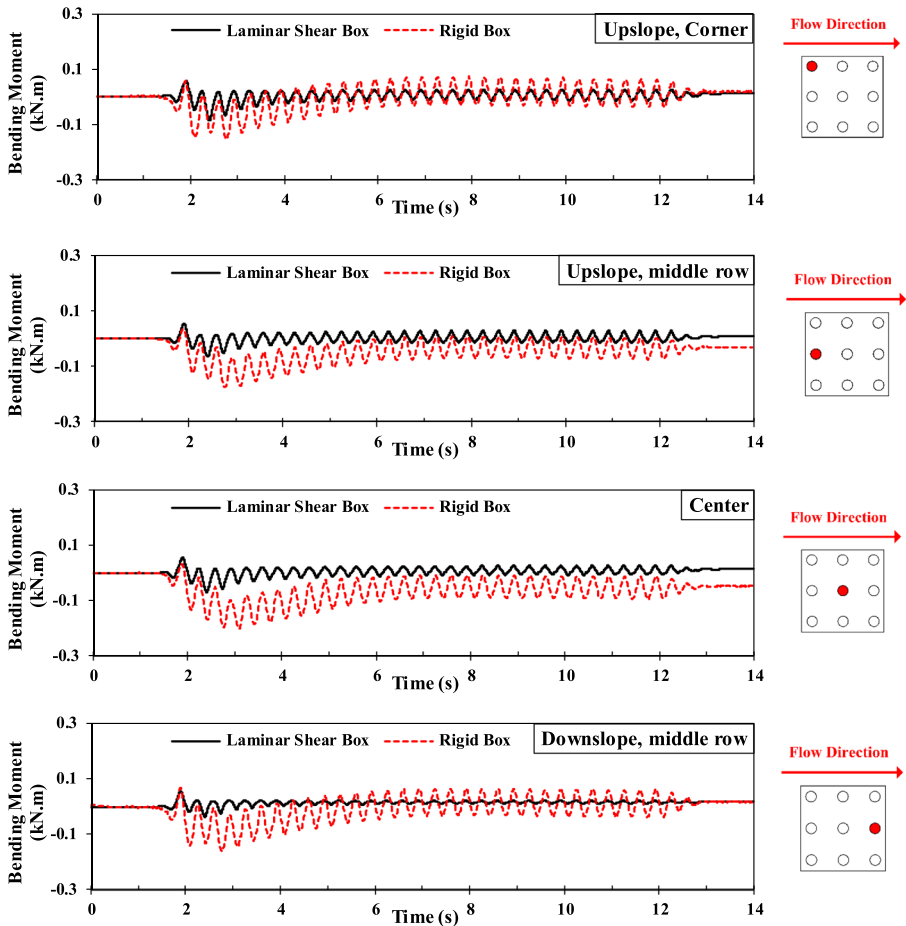
Fig. 8 Time histories of bending moments at lowest sections of the piles

box are between 1.7 and 2.9 times of those in the model with the laminar shear box, which is an indicator of the significant effect of the boundary conditions on the response.

The bending moments in the piles consist of monotonic and cyclic components. The cyclic and monotonic components of the bending moment represent inertial loading and kinematic loading from ground shaking and lateral spreading, respectively. Based on the observations in various earthquakes, lateral spreading does not occur coherently with the ground shaking, however, it happens after the earthquakes. Ironically, in physical modeling, inertial and lateral loadings happen almost simultaneously. Hence, the monotonic component of the bending moment, which is the kinematic part of the loading on piles should be extracted from the recorded values to assess the effects of lateral spreading on the piles. In order to obtain the time histories of the monotonic bending moment, the cyclic part of the total bending moment should be eliminated. For this purpose, the data were decomposed into cyclic and monotonic components. The cyclic component of the bending moment was obtained by passing the record through a high-pass filter and subsequently, the monotonic component of the bending moment was obtained using Eq. (1).
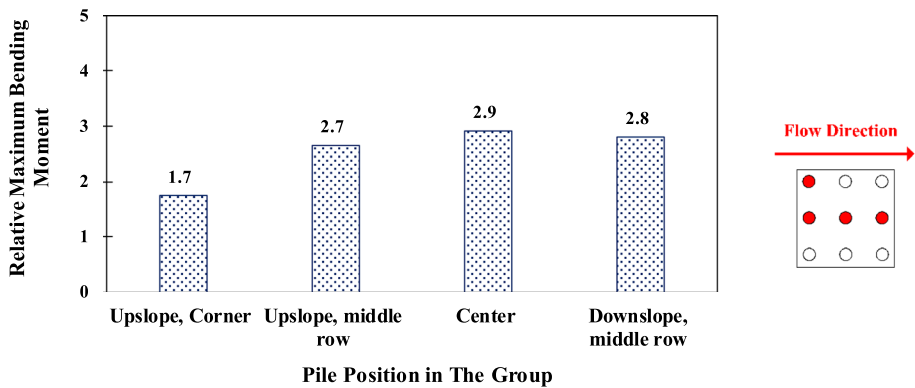
Fig. 9 Bar chart of the ratio of the maximum bending moments in the piles of the rigid box model to those of the laminar shear box model

$$M(t)_{monotonic} = M(t) - M(t)_{cyclic} \tag{1}$$

In the above equation, $M(t)_{monotonic}$ is the monotonic bending moment at the time of t, $M(t)$ is the total bending moment at the time of t, and $M(t)_{cyclic}$ is the cyclic bending moment at the time of t.

Figure 10 compares the time histories of the kinematic (monotonic) bending moments at the lowest sections of the corresponding piles in the models. As seen in Fig. 10, at the approximate time of 6.5 s- end of the 16th cycle of loading- the monotonic (kinematic) component of the bending moment remained constant. This can be attributed to the leveling off of the ground surface. In other words, the kinematic soil pressure on the piles was significantly decreased with the disappearance of the slope of the non-liquefiable surface layer. Because kinematic soil pressure and consequently kinematic bending moment are extremely dependent on the ground slope (in grounds without a quay wall). According to Fig. 10, the maximum kinematic bending moment on the pile groups occurred just after the onset of liquefaction. The relative maximum kinematic bending moments ($M_{max \text{ kinematic, model with rigid box}}$/ $M_{max \text{ kinematic, model with laminar shear box}}$) for different piles of the models are displayed in Fig. 11. The maximum kinematic bending moments experienced by piles in the model with the rigid box are between 2.9 to 6.4 times of those in the model with laminar shear box. Hence, the boundary condition affected the response of the piles in these experiments, significantly.

3.4.2 3.4.2. The effects of pile position in the groups

One of the notable points extracted from Figs. 8,9,10 and 11 is that piles in various positions of the groups exhibited different responses to lateral spreading. In other words, pile positions in the group affect the responses. Albeit, this subject is not considered in many guidelines (e.g., JRA 2002). In this section of the paper, several aspects of the effects of pile position in the group are revealed. According to Fig. 8, at the time of 2 s when liquefaction has not yet occurred, the maximum bending moments for downslope piles are rather higher than the corresponding piles in the upslope row of the groups. For instance, in the middle row of the group in the laminar shear box model, the bending moment of the downstream pile was 7% higher than the upstream pile, meaning that the ground cyclically
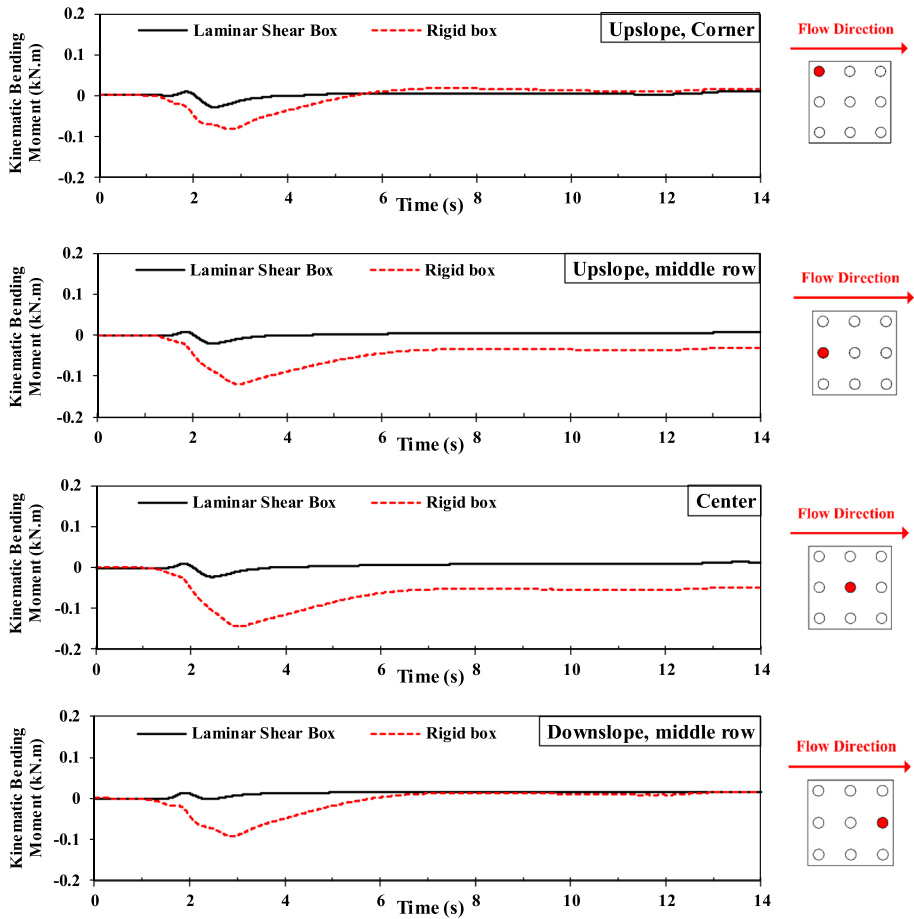
Fig. 10 Time histories of kinematic bending moments at lowest sections of the piles
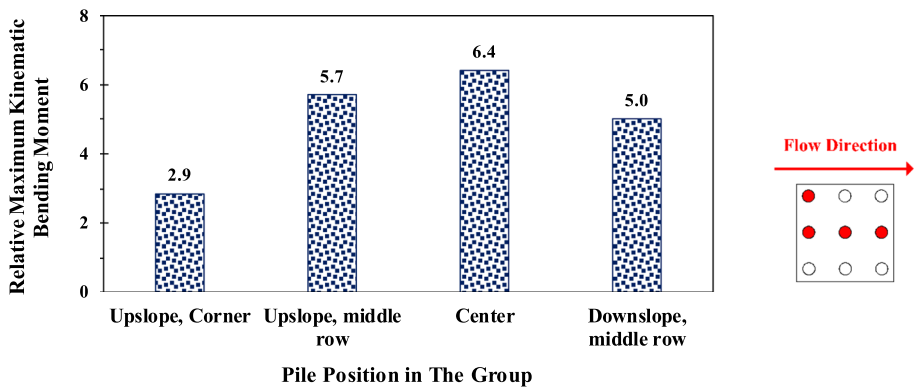

Fig. 11 Bar chart of the ratio of maximum kinematic bending moment of the piles in the rigid box mode to those in the laminar shear box model

moved toward the upslope of the model before liquefaction triggering. In other words, the downslope piles in the group protected the upslope piles in this before the liquefaction cycle of loading, or the upslope row acted as shadow piles, experiencing lower bending moments than the corresponding ones in the downslope row. This is in good agreement with the results of Ebeido et al. (2019a) who conducted shake table tests to study the behavior of 2×2 piles in a gently sloped ground. The results showed that the maximum bending moment occurred during the first few cycles of shaking, around the onset of liquefaction. Additionally, the downslope piles were subjected to higher bending moments than those for the upslope piles by approximately 20%.

According to Fig. 8, the maximum bending moment of the piles in the present study occurred approximately at the time of liquefaction triggering (2.5 s). The lateral movement of the liquefied soil toward the downslope leads to a downslope concave of the lowest part of the piles. This caused negative maximum bending moments in the piles. At this time, the bending moments in the piles in the upstream row were greater than those of the piles in the downstream row of the group because the soil mass upstream of the pile group moved more than that of downstream, due to lateral spreading. So, the piles in the downslope row, have been protected by the upslope piles, against the pressure excreted by the moving soil. For instance, in the middle row of the group in the laminar shear box model, the maximum bending moment of the upstream pile was 17% higher than that of the downstream one. This phenomenon known as "shadow effect" has been studied by several researchers (e.g., Haeri et al. 2012; 2021; He et al. 2008 and Tang et al. 2014). Haeri et al. (2021) conducted a case study using physical modeling, on a shake table to study the response of a 3×5 pile group in a mildly sloped ground to lateral spreading. The results showed that the maximum bending moments for the piles in the upslope row of the group were 23% to 40% higher than those for the piles in the downslope. Tang et al. (2014) conducted a shake table test to study the behavior of a 2×2 pile group behind a quay wall. In that research, the maximum bending moment of the rear piles (close to the quay wall) was approximately 30% higher than that for the front piles (far from the quay wall). This result shows that the lateral movement of the soil started from the downstream of the model, and the higher gradient of the soil pressure on the rear piles compared to that for the front piles has resulted in such an observation. Haeri et al. (2012) and He et al. (2008) conducted shake table tests to investigate the behavior of 2×1 pile groups without a cap in a gently sloping ground. In Haeri et al. (2012) research, the maximum bending moment for the upslope pile was approximately 16% higher than that for the downstream pile. The results of He et al. (2008) showed that the ratio of the maximum bending moment for the upslope pile to the downslope one was almost 2.64, which illustrates the importance of shadow effects on the responses of piles to lateral spreading.

According to Figs. 8 and 9, there is also a difference between the maximum bending moments at the middle and side rows of the pile groups. In the upstream row of the group in the model with the laminar shear box, the maximum bending moment for the middle pile was 28% more than that of the corner pile. It can be attributed to the neighboring effects. This is in good agreement with Haeri et al. (2012) who investigated this issue for a group of piles without a pile cap in a gently sloped ground without a crust layer. In that research, the middle pile of a 3×1 group experienced almost 37% less bending moment than the side pile. However, this phenomenon was not observed in the results of the experiment with the rigid box. It should be notable that the center pile in this test, experienced higher bending moments compared to the other piles in the middle row, and it might be postulated that in this experiment, the center pile resisted more, in the pile group, against lateral spreading. The difference between the maximum bending moment of the center pile

and the other piles was more than 10%. However, this result is somewhat inconsistent with the shadow effects in pile groups. In fact, in the first cycles of the loading, the bending moments of these piles were quite similar; however, with additional cyclic loading, the bending moment of the center pile became slightly greater than the other piles, specifically in the final cycles of the loading. Further observations might be required for a better understanding of the mechanism of this observation.

As mentioned in above Sect. 2, the pile spacing in this study was selected to be 3D (D=diameter) center to center. Some researchers have investigated the effects of pile spacing on the response of the pile groups to lateral spreading. In this line, Imamura et al. (2004) implemented a centrifuge experiment and concluded that when the pile spacing (center to center) was more than 4D to 5D, there were no interactions between the piles. Mao et al. (2019) conducted a series of shake table tests and showed that for the piles aligned in one row parallel to the direction of the slope with spacing less than 8D, the inner piles generally carried lower maximum bending moments than those of the front and rear piles. Mao et al. (2019) also observed that for 3×3 pile groups with different spacing (3.8D and 4D) the responses in the upslope piles were similar. Therefore, Mao et al. (2019) concluded that for the piles in the rows parallel and perpendicular to the ground slope direction, the group effects were not evident for the pile spacing larger than 8D and 3.8D, respectively.

3.5 Lateral force on the piles

The lateral forces on piles in physical modeling are usually back-calculated through the differentiation of distribution of bending moments along the piles. The data associated with the measured bending moments are discrete and most of the methods for differentiation of discrete data are not reliable. However, Brandenberg et al. (2010) proposed a method, which seems to be more reliable with minor errors applying finite element approximations, which is called Weighted Residual Method (WRM). The profile of lateral force on the piles due to lateral spreading is determined by the differentiation of the bending moment. In this way, piles are divided into several two nodded elements along pile length (L). The nodes are the sections where pair strain gauges are installed. Function $f(x)$, a polynomial function, is established for the bending moment along the depth of the pile. The direct calculation by differentiation of function $f(x)$ which can be named $f'(x)$ includes several errors. To minimize these errors, a function $g(x)$, is determined using WRM, as a representative of differentiation of the function $f(x)$. Then, the weighted residual function (ψ), which is the combination of various shape functions, is employed in order to minimize the difference between $g(x)$ and $f'(x)$. The first differentiation of the bending moment, namely shear force, can be determined by employing appropriate shape functions and solving Eq. (2).

$$\int_0^L \{g(x) - f'(x)\}.\psi(x)dx = 0 \tag{2}$$

To determine the kinematic lateral forces induced by lateral spreading on the piles, the cyclic component was eliminated from the beck-calculated values. The maximum kinematic lateral shear forces exerted on the piles of both models due to lateral spreading are calculated using this method, as shown in Fig. 12. It should be noticed that the maximum kinematic lateral forces on the piles were imposed on the lowest section of them, i.e., the boundary of the liquefiable and the underlying non-liquefiable layer

(depth = 138 cm according to Fig. 3a). According to this figure, kinematic lateral shear forces induced by lateral spreading on the piles in the liquefiable layers are greater than those in the crust layers; which can be attributed to the effects of the thickness of the layers. The small values of the lateral force applied from both crust and liquefiable layers on the center piles in both experiments are notable as well. It is in contrast with the measured bending moments in the center piles, which have been the most critical ones in both models. Such a significant apparent behavioral difference between the values of the calculated lateral forces and the measured bending moments can be attributed to the effects of the derivation of the bending moment profiles having different signs along the length of the piles for the calculation of kinematic lateral forces. Also comparing the maximum kinematic forces in the upslope corner and the middle row of the piles confirms the neighboring effects on the piles of a group subjected to lateral spreading. The piles in the middle row of the upslope piles of the groups experienced less force compared to the piles in the corners in both models, being protected by the corner piles. In both models, the maximum kinematic forces in the downslope piles of the middle rows were slightly more than those of the upslope piles of the same row. This issue can be attributed to the higher lateral movement of the soil mass in the downslope of the models and soil-pile separation near the ground surface. Significant differences in
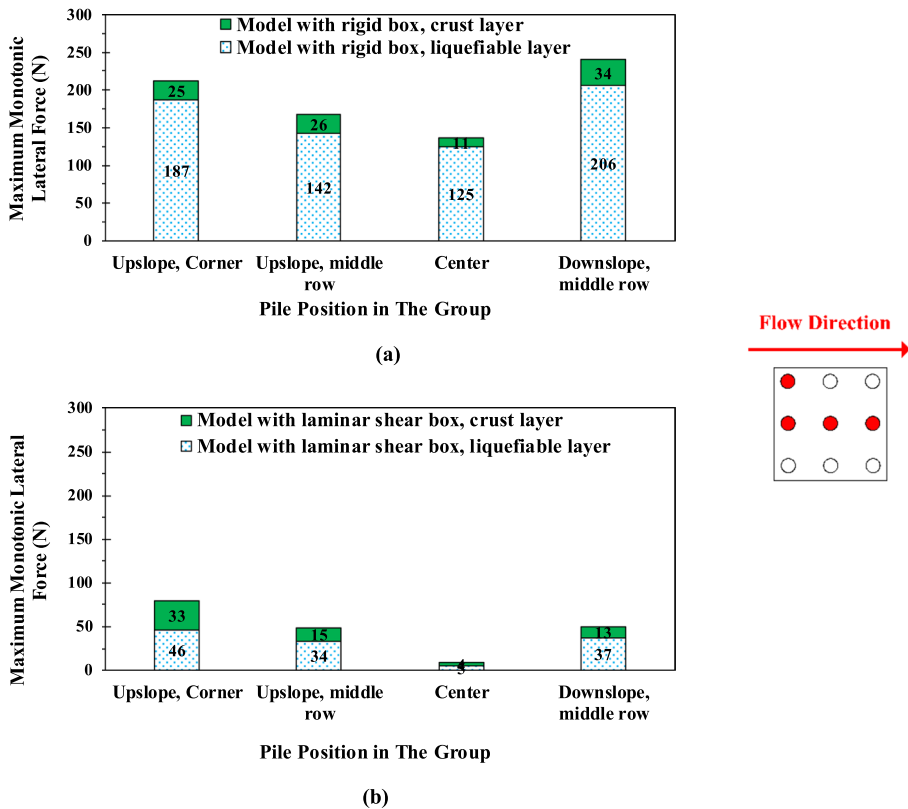

Fig. 12 Maximum kinematic forces on the piles in the experiments: **a** the model with the rigid box, and **b** the model with the laminar shear box

the values of the lateral forces on the piles, corresponding to each model and the piles within each group of the models are notable. The effect of the pile's position in a group and the effect of the boundary conditions on the response of the pile groups to lateral spreading can remarkably be observed from Fig. 12; the fact that the method proposed by JRA (2002) disregards it.

3.6 Visual observations during and after the experiments

Several professional cameras were employed to record the models from various viewpoints before, during, and after the shaking. One of the most important and useful cameras recorded the ground surface from just above the models. Some snapshots recorded by this camera for the rigid and laminar box models are exhibited in Figs. 13 and 14, respectively. These photos were analyzed and evaluated to obtain the patterns of the lateral soil displacement of the ground surface before, during, and after liquefaction and lateral spreading. Figures 13a and 14a show the model's surface at the end of construction and before shaking. As seen in these figures, square meshes were constructed using colored sand to better observe and analyze the lateral soil movements during, and after the shakings. Figures 13b and 14b show tension cracks generated in the upslope of the model's surfaces during the shaking. Lateral spreading caused tension cracks mainly perpendicular to the direction of the sloped ground. Similar tension cracks due to lateral spreading have been observed by other researchers, e.g., tension cracks in the ground near the piers of the Nishinomiya bridge due to lateral spreading in the Kobe 1995 earthquake (UC Davis, Civil and Environmental Engineering). In Figs. 13c and 14c, the sand boils are visible at several points of the models' surfaces, most of them occurring after the shakings. In fact, sand boils occurred concurrently with the upward dissipation of excess pore water pressure, generated due to the liquefaction of liquefiable layers during the shaking, however, breaking through the crust and boiling through cracks and fissures mainly started after the shaking.

The patterns of the surface displacement of the models were recorded and analyzed by image processing of the deformed meshes at the ground surfaces, as shown in Fig. 15. Initial and final positions of the lines associated with the meshes at the ground surfaces are demonstrated with black and red lines, respectively. As seen in Fig. 15, the amounts of the maximum surface displacement for the model with the laminar shear box and the model with the rigid box were 46 mm and 50 mm (equal to about 370 mm and 400 mm at the prototype scale), respectively. Note that the maximum lateral displacement of the soil occurred at the upstream parts of both models. According to the results of the displacement sensor installed in the free field, the maximum displacement of the ground surface was about 32 mm (equal to about 260 mm at the prototype scale).

It should also be noted that the ground subsidence due to the shakings was measured after the full dissipation of excess pore water pressure. On this basis, the new relative density of the liquefiable layer was calculated assuming that the non-liquefiable layers have not been densified by shakings due to the cohesion or high density. The slope of the ground surface disappeared in both models due to lateral spreading. Based on these measurements and the results of image processing, it was deduced that the new value of the relative density of the liquefiable layer in the rigid box model was 48% and that in the laminar shear box model was 33%. These findings also proved the effects of the rigid wall wave reflection on the response of the physical model, which resulted in denser or more compacted liquefiable soil when compared with those of the laminar shear box model.
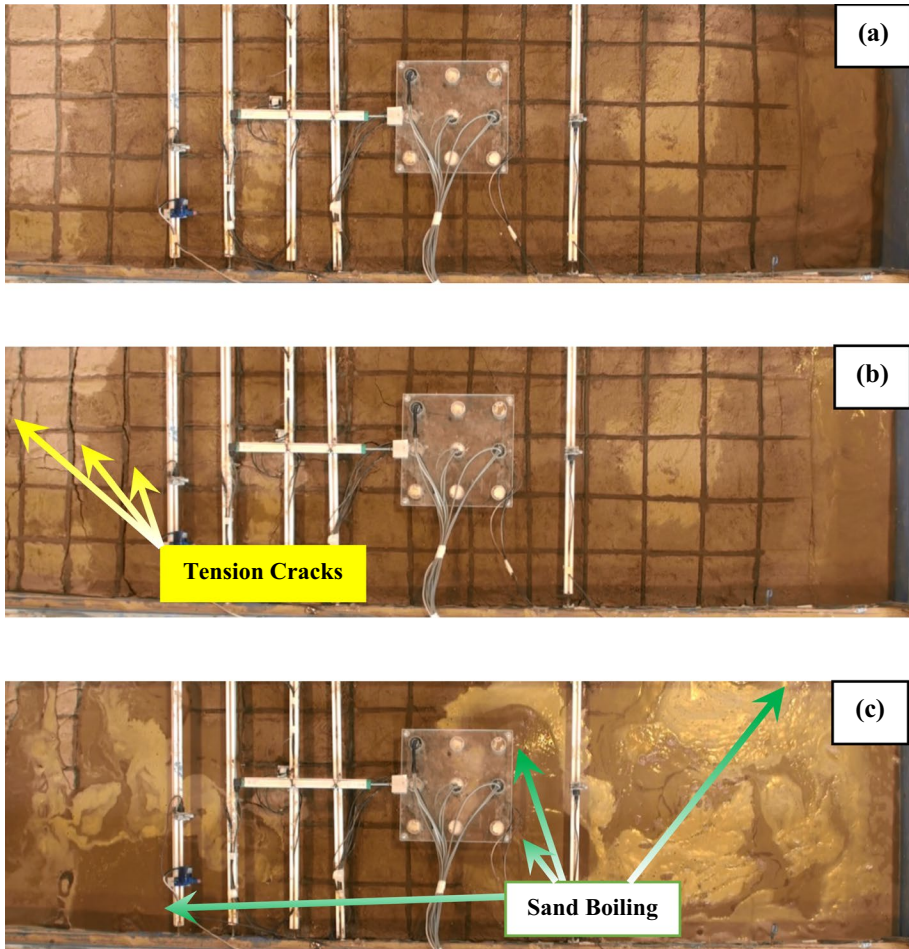
Fig. 13 Top view photos of the model with the rigid box: **a** the model before shakings, **b** tension cracks during shaking, and **c** sand boiling after shaking

4 Comparing the test results with design methods

Two practical methods to design piles against lateral spreading are known as: (a) the force based method, and (b) the displacement based method. In this paper, the ability of these methods to predict the responses of piles in a pile group to lateral spreading is evaluated.

4.1 Force based method

One of the prominent methods for the design of piles against lateral spreading effects is suggested by JRA (2002). In this method, as a force-based method, the effects of liquefaction-induced lateral spreading on piles are evaluated by indicating the pressures diagram, induced by lateral spreading on the piles. JRA (2002) suggests that the lateral spreading

Fig. 14 Top view photos of the model with the laminar shear box: **a** the model before shaking, **b** tension cracks during shaking, and **c** sand boiling after shaking
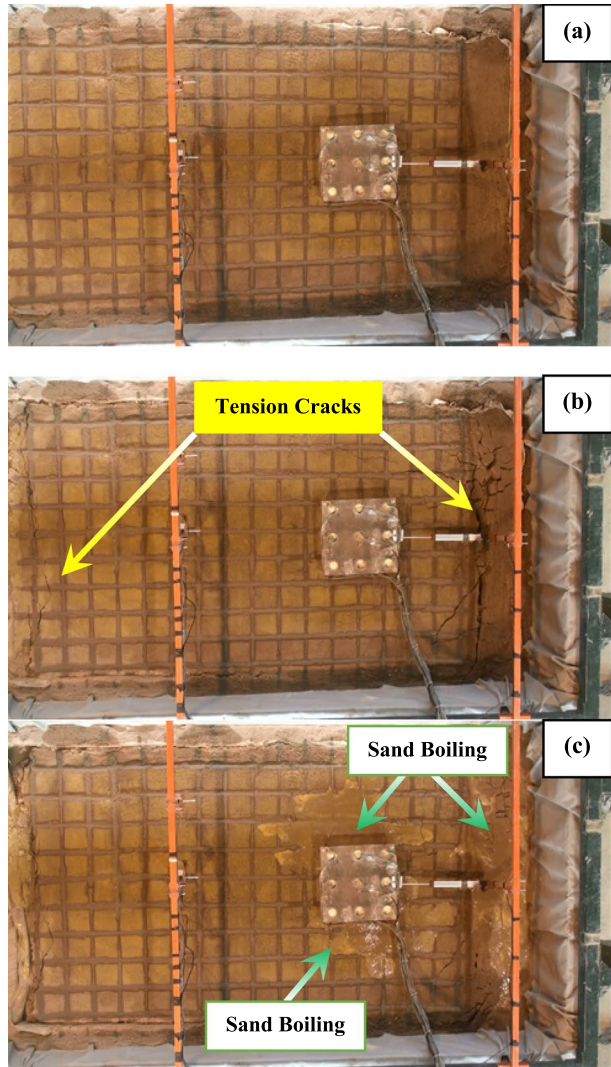
pressure on the piles in a liquefiable layer is equal to 30% of the total vertical stress at each depth, while the associated pressure on the piles in a non-liquefiable crust layer is equal to the passive pressure at each depth of the crust layer. Pile groups are considered as a single pile with an outer width of the group according to JRA (2002) and each pile bears equal pressure by dividing the total pressure by the number of piles.

In this study, profiles of the soil pressure on the piles were determined by the second differentiation of bending moment or the first differentiation of lateral force. The first differentiation of the bending moment, namely shear force, was determined by employing appropriate shape functions and solving Eq. (2) as explained in Sect. 3.5 the nodes are the sections where pair strain gauges are installed. Functions $f(x)$ and $f'(x)$, polynomial functions, were established for the kinematic bending moment and kinematic lateral force along the depth of the pile, respectively. The direct calculation by differentiation of function $f'(x)$
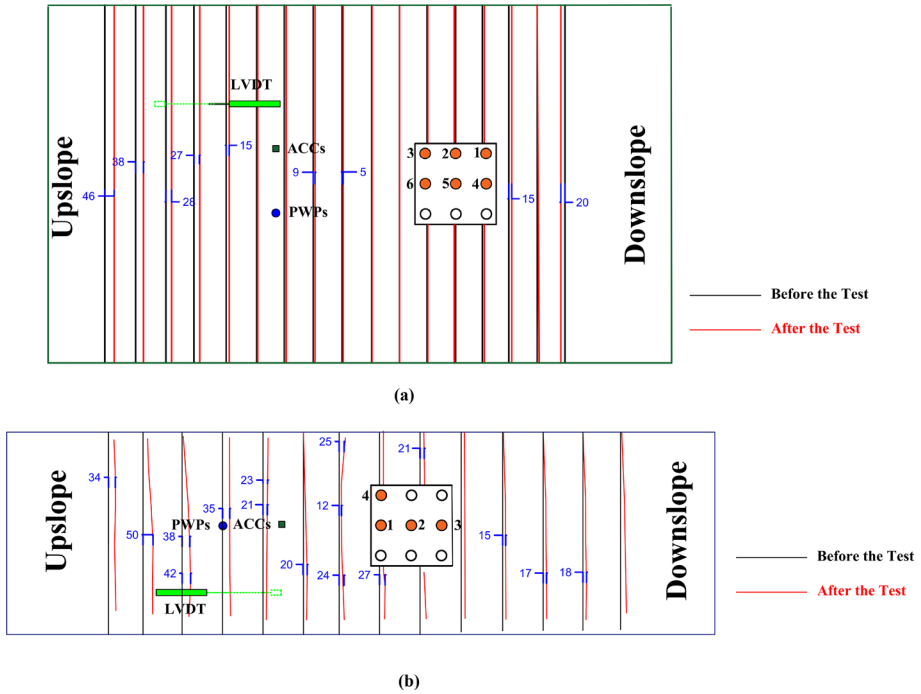
Fig. 15 Patterns of surface displacements obtained by image processing for: **a** the model with the laminar shear box, and **b** the model with the rigid box. (Black lines: initial position of the mesh lines, red lines: final position of the mesh lines, units = mm)

which can be named $f''(x)$ also includes various errors. Hence in the same line, as presented in Sect. 3.5, the WRM method which was suggested by Brandenberg et al. (2010) is implemented. To minimize these errors, a function $h(x)$, is determined, as a representative of differentiation of the function $f'(x)$. The weighted residual function (ξ), which is a combination of various shape functions, is employed in order to minimize the difference between $h(x)$ and differentiation of the functions $f'(x)$ or f''. Equation (3) was solved for these functions, and finally, the kinematic soil pressure exerted by lateral spreading was determined.

$$\int_0^l \{h(x) - f''(x)\}.\xi(x)dx = 0 \tag{3}$$

In this paper, the pile located in the upstream corner of the group was selected to compare the effects of boundary conditions on the induced lateral pressures on piles of the models. Profiles of kinematic pressure along the upstream corner pile at different times during and after the shakings are displayed in Fig. 16a. According to this figure, soil pressure increased after liquefaction triggering in the 2nd cycle of the loading, and it decreased after the 4th cycle of the loading. The maximum values of soil pressure were applied in the 4th cycle of the loading, which corresponds to the onset of lateral spreading of the liquefiable ground. The profiles of the soil pressures after the shakings, exhibited in Fig. 16a, show minor residual (final) pressures on the piles in both models. The maximum kinematic soil pressures, back calculated from the experiments, are compared with those estimated

by JRA (2002) in Fig. 16b. It should be noted that JRA (2002) suggests an identical distribution of the soil pressure on all the piles of a group, neglecting shadow and neighboring effects on piles. According to Fig. 16b, the center pile in both models experienced minor pressure along the total depths of the piles due to neighboring and shadow effects. The results of the present study illustrate that the position of piles in a group is important when the lateral spreading pressure on the piles is calculated and is recommended to be considered in pile design against lateral spreading in important projects. Other studies also detected similar observations, e.g., Motamed et al. (2007; 2010), Motamed and Towhata (2010), He et al. (2008), Haeri et al. (2012, 2014), Tang et al. (2014), Liu et al. (2017), Li and Motamed (2017), Kavand et al. (2014; 2021). For instance, Liu et al. (2017) conducted a shake table test to investigate the effects of lateral spreading on a 2×2 pile group in a liquefiable ground without a non-liquefiable crust layer. The results showed that the liquefied soil pressure on the rear pile (near the quay wall) was approximately twice of that of the front pile (far from the quay wall).

Figure 17 compares the maximum kinematic forces on the corresponding piles of both models with the estimated value using JRA (2002) recommendation. According to this figure, there is a good agreement between the lateral kinematic forces estimated by JRA (2002) and the results of the rigid box model. However, lateral kinematic forces results from the laminar shear box model are much less than those obtained from either the rigid
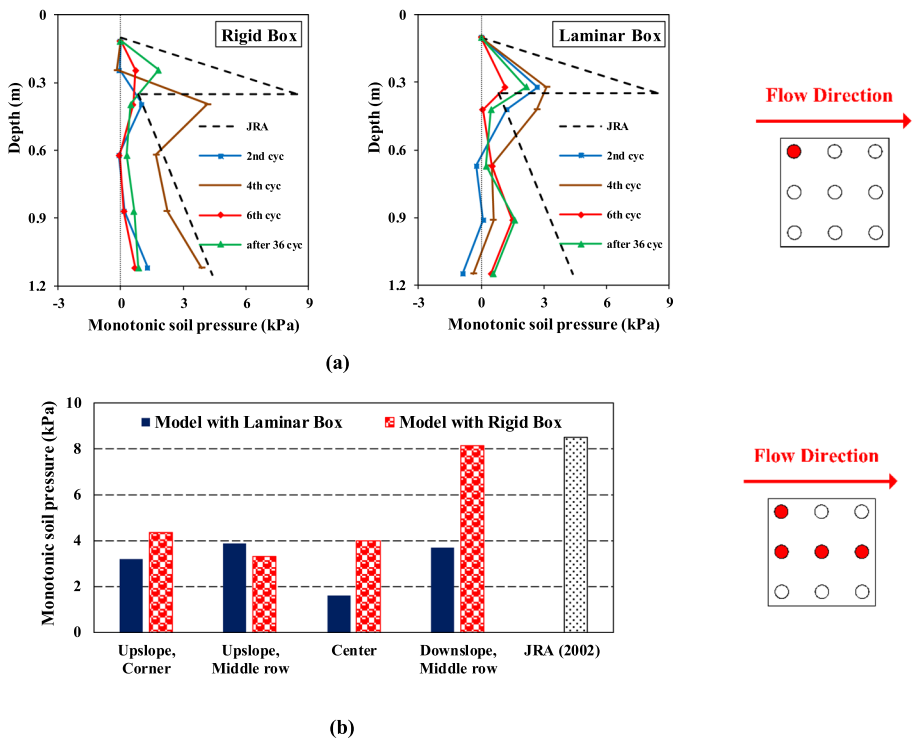

(a)

(b)

Fig. 16 Comparison of kinematic soil pressure in two different boxes: **a** profile of kinematic soil pressure on the corner piles, and **b** maximum kinematic pressure on the piles, back calculated from the results of the experiments and that estimated by JRA (2002)

box model or estimated by JRA (2002). Most of the results reported by others are also not in line with the JRA (2002). For instance, Motamed et al. (2008, 2010) conducted shake table tests on 3×3, 6×6, and 11×11 pile groups in liquefiable gently sloped grounds, Motamed and Towhata (2010) performed shake table tests on 3×3 pile groups without and with cap, and Motamed et al. (2009) who conducted shake table test on a 2×2 pile group behind a quay wall also revealed that JRA (2002) underestimated the lateral force associated with lateral spreading on the tested piles; especially for the rear row piles. In contrast, the results of Liu et al. (2017) showed that in a liquefiable sloping ground without a non-liquefiable crust layer the bending moments experienced by the piles of a 2×2 group were less than those predicted by JRA (2002). These results reveal that many factors (e.g., ground slope, pile cap, group effects and boundary conditions) affect the soil-pile interaction which is not considered by JRA (2002). However, JRA (2002) is a straightforward and practical code to design piles against lateral spreading with admissible accuracy and convenient simplicity.

The profile of the maximum monotonic bending moments of the upstream corner piles in both experiments is compared to that predicted using JRA (2002) in Fig. 18. According to this figure, the JRA design code acceptably predicted the bending moment profile of the pile in the rigid box model, but overestimated the response of the pile in the laminar shear box model. The ratio of the maximum kinematic bending moments in the models with rigid and laminar shear boxes to the JRA (2002) predicted values were 26% and 110%, respectively.

4.2 Displcement based method

In the displacement based method, a Beam on Nonlinear Winkler Foundation (BNWF) model is employed to design piles against liquefaction induced lateral spreading. In this approach, the profile of the ground displacement is applied to separate springs that represent the ground. The monotonic pressure-relative displacement (p-y) curves suggested by API (2002) can be used to obtain the stiffness of the springs in non-liquefiable layers. A reduction factor known as the p-multiplier should be used to obtain the stiffness of the springs in the liquefied layer. Different approaches to obtain the p-multiplier have been suggested by the researchers and codes, e.g., Bandenberg (2005) and AIJ (2001), see Fig. 19a. In this approach, the p-multiplier can be estimated based on the corrected blow count of standard penetration test (SPT). The corrected SPT blow count, $(N_1)_{60}$, for the
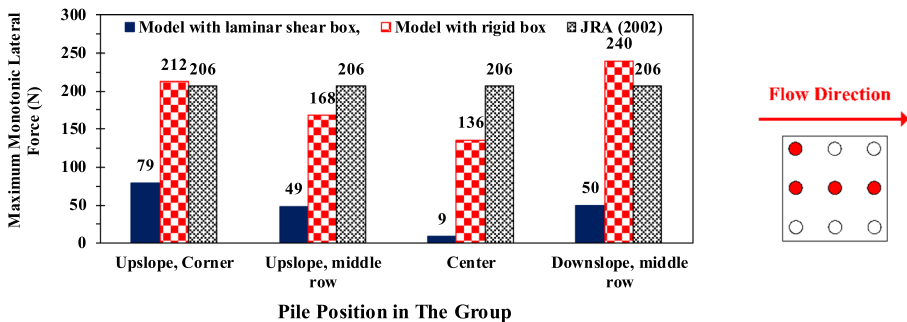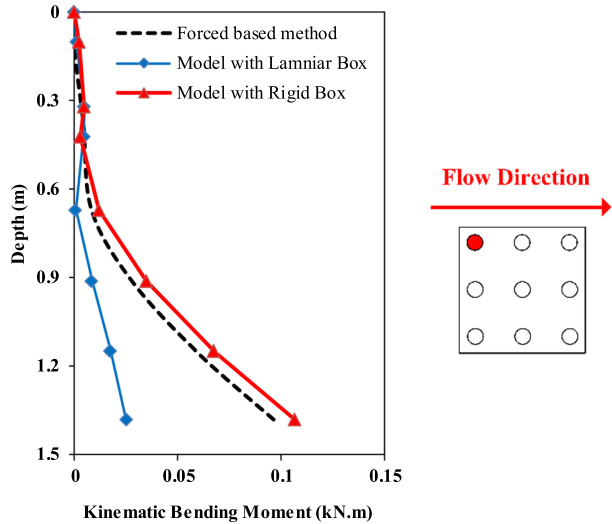

Fig. 17 Maximum kinematic forces on the piles back calculated from the results of the experiments and that estimated by JRA (2002)

Fig. 18 Profiles of the kinematic bending moment for the upstream corner pile

very loose sand was assumed to be 4, using Bowles (1997). According to the graphs in Fig. 19 a, for the sand layer with $(N_1)_{60}=4$, constructed in the models of this study, the p-multiplier can be considered as 0.064. The p-y curves for the present models predicted from the displacement based method are exhibited in Fig. 19b.

In the present study, the p-y curves for the piles at different times were determined. It should be noted that y is the relative displacement of soil and pile, which can be derived from the difference between the ground displacement (y_g) and the pile displacement (y_p). As seen in Fig. 1a, transparent plexiglass windows existed on one of the walls of the rigid box to observe the soil lateral displacement during the tests. A number of the colored vertical sand column were also built adjacent to the plexiglass wall during model construction to observe and measure the values of the lateral spreading in various points of the soil mass. The profile of lateral soil displacement in the rigid box model was obtained as
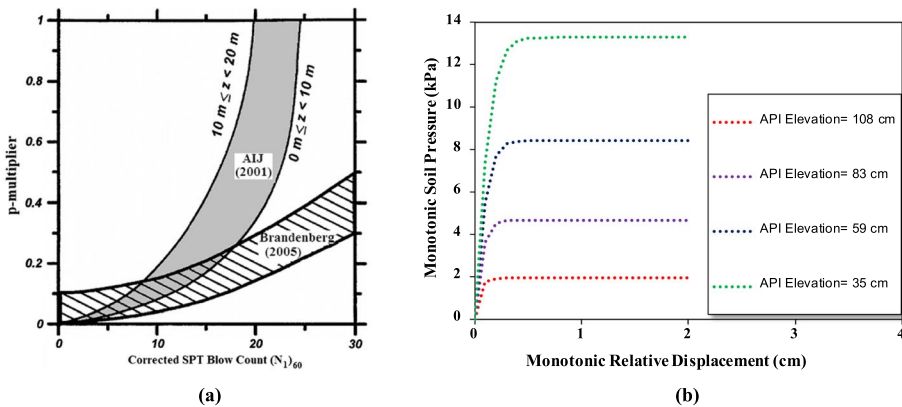

Fig. 19 Displacement based method: **a** Suggested p-multiplier in different references, AIJ (2001) and Brandenberg (2005), and **b** predicted p-y curves for the models based on displacement based method with p-multiplier = 0.064

demonstrated in Fig. 20. As seen in this figure, the location of the initial and final situations of the colored sands can indicate the soil lateral displacement profiles. According to Fig. 20 and also based on suggestions by Towhata (2008) and Haeri et al. (2012), a sine function with respect to the depth was assumed for the soil displacement profile due to lateral spreading in liquefied soil, as given in Eq. (4). Towhata (2008) showed that the lateral displacement of liquefiable layer changes is in a harmonic manner in the vertical direction, while the surface crust moves along with the liquefied subsoil. Hence, it is possible to express the lateral displacement of the liquefiable layer as a sin function of the elevation. Similarly, Haeri et al. (2012) conducted a shake table experiment with the same rigid box and observed a sinusoidal soil displacement profile in the liquefiable layer due to lateral spreading. It should be noticed that some irregularities can be observed in the shape of the colored sand in Fig. 20. It happened because of the remained glue keeping the half-pipe filled with gray sand from the intrusion of yellow sand during liquefiable sand sedimentation. When the half pipe was removed from the rigid container, the strip glues remained on the plexiglass in some cases and caused a frictional surface for free movement of the gray sand.

$$y_g(z.t) = D_{gs}(t) \sin \frac{\pi(z - B)}{2H} \tag{4}$$

In the above equation, y_g (z, t) is the free field soil displacement of the liquefiable layer at time t and elevation z from the bottom of the soil profile, $D_{gs}(t)$ is the surface displacement of the liquefiable layer in the free field at time t, H is the thickness of the liquefiable layer, and B is the thickness of the base layer of the soil profile. In this study, Eq. (4) was employed to estimate the soil displacement profile due to lateral spreading in the free field of the rigid box model. The profile of the soil lateral movement in the laminar shear box model was detected through the continuous recording of the movement of the laminates. The movement of the laminar shear box was obtained using a video, recorded from the sidewall of the box during the experiment. The lateral
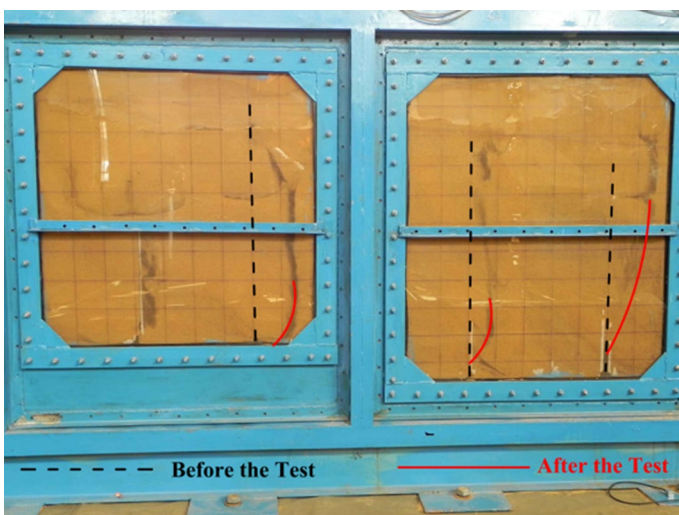

Fig. 20 Lateral movement of the colored sand columns in the rigid box model due to lateral spreading

movement of the liquefiable soil layer in the laminar shear box model was linear with depth in this study, as was expected. In both models, it was assumed that the crust layer slipped over the liquefiable layer during lateral spreading due to its cohesive nature. It should be noted that the base layer was a dense non-liquefiable layer that was stiff enough to experience no soil displacement during the shakings.

The piles displacements (y_p) were determined using Eq. (5). In this equation, y_{pile} is the pile displacement, M is the bending moments, EI is the flexural rigidity of the pile, and z is the considered depth. Two boundary conditions are required to solve Eq. (5): (1) zero displacement at the bottom of the pile, and (2) pile head displacement measured by LVDT attached to the pile cap.

$$\frac{d^2}{d_z^2} y_{Pile} = \frac{M}{EI} \tag{5}$$

The p-y curves for the upstream corner pile obtained in the experiments and predicted by the displacement based method are compared in Fig. 21a. As seen in this figure, the response of the pile to lateral spreading was more intense in the model with the rigid box, which can be attributed to the effects of boundary conditions. The shapes of back-calculated and obtained p-y curves in the model with the laminar shear box are consistent. However, the p-y curves are overestimated for both experiments. As presented in Fig. 21b, suitable p-multipliers for the models with rigid and laminar shear boxes were back-calculated to be 0.035 and 0.015, respectively.

5 5. Summary and Conclusions

In this paper, the effects of boundary conditions on the response of 3×3 pile groups in gently sloped ground to lateral spreading using shaking table were investigated. For this purpose, a large rigid box and a large laminar shear box were designed and constructed. In addition, two identical physical models (except for the boundary condition) were built and tested on a shake table under identical shakings. Based on the authors' knowledge, this study is unique from this point of view, as it compares the results of two different complicated physical models of piles in liquefiable soil subjected to lateral spreading, with identical conditions except for the boundary conditions. The main conclusions of this study are as follows:

1. The acceleration at the ground surface for the laminar shear box model was attenuated after liquefaction, but the surface acceleration for the rigid box model behaved differently, even after the liquefaction.
2. The maximum displacement of the pile cap in the rigid box model was much more than that for the laminar shear box model.
3. The results of image processing and displacement transducers showed that the ground surface of the rigid box model experienced greater lateral movement compared to that in the laminar shear box model.
4. The maximum values of the total and monotonic (kinematic) bending moments for the piles in the rigid box model were significantly greater than those in the laminar shear box model.
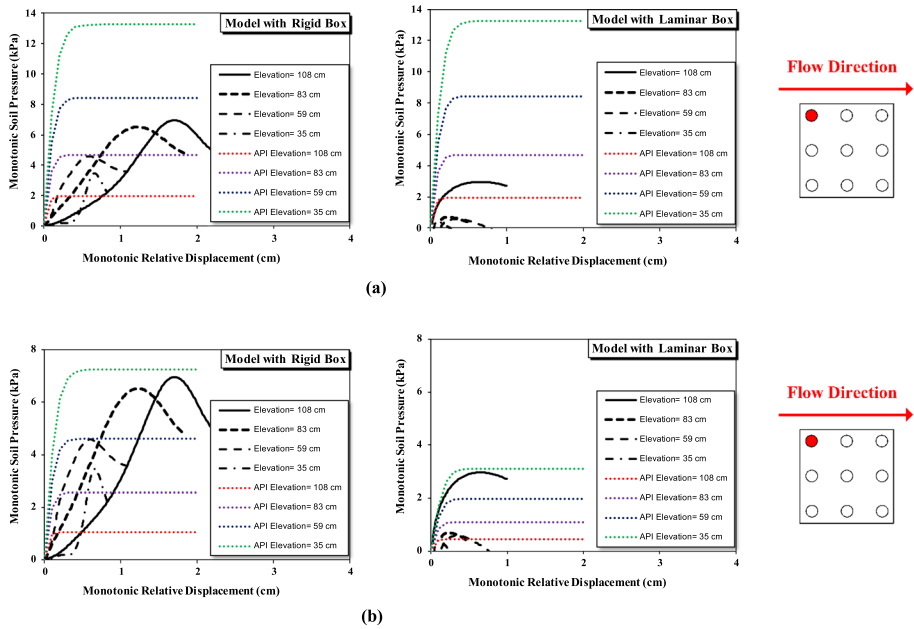
Fig. 21 p-y curves for the upstream corner pile: **a** with the p-multiplier = 0.064 for the models, and **b** with the p-multiplier = 0.035 for the rigid box model and the p-multiplier = 0.015 for the laminar box model

5. The maximum monotonic lateral forces of all piles of the rigid box model were close to the values predicted by JRA (2002), but were much higher than those obtained from the laminar shear box model.

Author contributions SMH initiated the study conception and fund raise, and leaded and contributed to the design, operation and analysis of the data. MR, SS and AK contributed in material and model preparation, operation, data collection and analysis. All other authors contributed in the model preparation and operation of the tests. SMH and MR prepared the first draft of the manuscript. All authors commented on previous versions of the manuscript and approved the final one.

Data availability The datasets analyzed during the current study are available from the corresponding author on reasonable request.

Declarations

Conflict of interest The authors declare that they have no known competing financial interests or personal relationships that could have appeared to influence the work reported in this paper.

References

Abdoun T, Dobry R, O'Rourke T, Goh SH (2003) Pile response to lateral spreads: centrifuge modeling. J Geotech Geoenviron Eng 129(10):869–878. https://doi.org/10.1061/(ASCE)1090-0241(2003)129:10(869)

AIJ, Architectural Institute of Japan (2001) Recommendations for Design of Building Foundations (in Japanese).

API, Recommended Practice for Planning Design and Constructing Fixed Offshore Platforms (2000) 20th Ed. Washington, DC.

Ashford SA, Juirnarongrit T, Sugano T, Hamada M (2006) Soil-pile response to blast-induced lateral spreading i: field test. J Geotech Geoenviron Eng 132(2):152–162. https://doi.org/10.1061/(ASCE)1090-0241(2006)132:2(152)

Bhattacharya S, Lombardi D, Dihoru L, Dietz MS, Crewe AJ, Taylor CA (2012) Model container design for soil- structure interaction studies. In: Fardis MN, Rakicevic ZT (eds) Role of seismic testing facilities in performance-based earthquake engineering. Geotechnical, Geological and Earthquake Engineering. Springer Science

Bhattacharya S, Sarkar R, Huang Y (2013) Seismic Design of Piles in Liquefiable Soils. In: Huang Y, Wu F, Shi Z, Ye B (eds) New frontiers in engineering geology and the environment. Springer Geology. Springer, Berlin, Heidelberg

Bowles JE (1997) Foundation Analysis and Design. The McGraw-Hill Companies

Brandenberg SJ, Wilson DW, Rashid MM (2010) Weighted residual numerical differentiation algorithm applied to experimental bending moment data. J Geotech Geoenviron Eng 136(6):854–863. https://doi.org/10.1061/(ASCE)GT.1943-5606.0000277

Brandenberg SJ (2005) Behavior of pile foundations in liquefied and laterally spreading ground. PhD thesis, University of California at Davis, CA

Chang D, Boulanger R, Brandenberg S, Kutter B (2013) FEM analysis of dynamic soil-pile structure interaction in liquefied and laterally spreading ground. Earthq Spectra 29(3):733–755. https://doi.org/10.1193/1.4000156

Coduto DP (2001) Foundation Design Principles and Practices. Prentice Hall, Upper Saddle River, New Jersey

Dobry R, Abdoun T, O'Rourke TD, Goh SH (2003) Single piles in lateral spreads: field bending moment evaluation. J Geotech Geoenviron Eng 129(10):879–889. https://doi.org/10.1061/(ASCE)1090-0241(2003)129:10(879)

Ebeido A, Elgamal A, Tokimatsu K, Abe A (2019a) Pile and pile-group response to liquefaction-induced lateral spreading in four large-scale shake-table experiments. J Geotech Geoenviron Eng 145(10):04019080. https://doi.org/10.1061/(ASCE)GT.1943-5606.0002142

Ebeido A, Elgamal A, Zayed M (2018) Pile response during liquefaction-induced lateral spreading: 1-g shake table tests with different ground inclination. Physical Modelling in Geotechnics. London, Taylor & Francis Group. https://doi.org/10.1201/9780429438646-90.

Ebeido A, Elgamal A, Zayed M (2019b) Large scale liquefaction-induced lateral spreading shake table testing at the university of california San Diego. In: Proceedings of 8th international conference on case histories in geotechnical engineering (Geo-Congress 2019b). Philadelphia, Pennsylvania.

Finn WDL, Ledbetter RH, Wu G (1994) Liquefaction in Silty Soils: Design and Analysis. Geotech Spec Pub 44:51–76

Gonzalez L, Abdoun T, Dobry R (2009) Effect of soil permeability on centrifuge modeling of pile response to lateral spreading. J Geotech Geoenviron Eng 135(1):62–73. https://doi.org/10.1061/(ASCE)1090-0241(2009)135:1(62)

Haeri SM, Kavand A, Rahmani I, Torabi H (2012) Response of a group of piles to liquefaction-induced lateral spreading by large scale shake table testing. Soil Dyn Earthq Eng 38:25–45. https://doi.org/10.1016/j.soildyn.2012.02.002

Haeri SM, Kavand A, Asefzadeh A, Rahmani I (2013) Large scale 1g shake table model test on the response of a stiff pile group to liquefaction induced lateral spreading. In: Proceedings of the 18th international conference on soil mechanics and geotechnical engineering. Paris, France

Haeri SM, Kavand A, Raisianzadeh J, Padash H, Rahmani I, Bakhshi A (2014) Observations from a large scale shake table test on a model of existing pile-supported marine structure subjected to liquefaction induced lateral spreading. In: Proceedings of 2nd European conference on earthquake engineering and seismology. Istanbul, Turkey.

Haeri SM, Rajabigol M, Sayaf H, Salaripour S, SeyedGhafouri SMH, Kafashan F, Khoshnoud A (2019) Response of 2×2 pile groups to soil liquefaction in inclined base layer: 1g shake table tests. In: Proceedings of 8th international conference on seismology and earthquake engineering. Tehran, Iran.

Haeri SM, Rajabigol M, Moradi M, Zangeneh M (2021) A case study of dynamic response of a 3×5 pile group to liquefaction induced lateral spreading: 1g shake table test. In: Proceedings of 12th international congress on civil engineering. Mashhad, Iran.

Hamayoon KH, Morikawa Y, Oka R, Zhang F (2016) 3D dynamic finite element analyses and 1g shaking table tests on seismic performance of existing group-pile foundation in partially improved grounds under dry condition. Soil Dyn Earthq Eng 90:196–210. https://doi.org/10.1016/j.soildyn.2016.08.032

He L, Elgamal A, Abdoun T, Abe A, Dobry R, Hamada M, Meneses J, Masayoshi S, Shantz T, Tokimatsu K (2009) Liquefaction-induced lateral load on pile in a medium Dr sand layer. J Earthquake Eng 13(7):916–938. https://doi.org/10.1080/13632460903038607

He L, Ramirez J, Lu J, Tang L, Elgamal A, Tokimatsu K (2017) Lateral spreading near deep foundations and influence of soil permeability. Can Geotech J 54(6):846–861. https://doi.org/10.1139/cgj-2016-0162

He L, Elgamal A, Hamada M, Meneses J (2008) Shadowing and Group Effects for Piles during Earthquake-Induced Lateral Spreading. In: Proceedings of the 14th World Conference on Earthquake Engineering. Beijing, China

Iai S (1989) Similitude for shaking table tests on soil–structure–fluid model in 1g gravitational field. Soils Found 29(1):105–118. https://doi.org/10.3208/sandf1972.29.105

Iai S, Tobita T, Nakahara T (2005) Generalized scaling relations for dynamic centrifuge tests. Geotechnique 55(5):355–362. https://doi.org/10.1680/geot.2005.55.5.355

Imamura S, Hagiwara T, Tsukamoto Y, Ishihara K (2004) Response of pile groups against seismically induced lateral flow in centrifuge model tests. Soils Found 44(3):39–55. https://doi.org/10.3208/sandf.44.3_39

JRA Japan Road Association (2002) Seismic Design Specifications for Highway Bridges, English version, Prepared by Public Works Research Institute (PWRI) and Ministry of Land. Tokyo, Japan: Infrastructure and Transport.

Juirnarongrit T, Ashford SA (2006) Soil-pile response to blast-induced lateral spreading II: analysis and assessment of the p–y method. J Geotech Geoenviron Eng 132(2):163–172. https://doi.org/10.1061/(ASCE)1090-0241(2006)132:2(163)

Kavand A, Haeri SM, Asefzadeh A, Rahmani I, Ghalandarzadeh A, Bakhshi A (2014) Study of the behavior of pile groups during lateral spreading in medium dense sands by large scale shake table test. Int J Civil Eng 12(3):374–439

Kavand A, Haeri SM, Raisianzadeh J, SadeghiMeibodi A, AfzalSoltani S (2021) Seismic behavior of a dolphin-type berth subjected to liquefaction induced lateral spreading: 1g large scale shake table testing and numerical simulations. Soil Dyn Earthq Eng 140:106450. https://doi.org/10.1016/j.soildyn.2020.106450

Kim H, Kim D, Lee Y, Kim H (2020) Effect of soil box boundary conditions on dynamic behavior of model soil in 1 g shaking table test. J Appl Sci 10:4642. https://doi.org/10.3390/app10134642

Knappett JA, Madabhushi SPG (2012) Effects of axial load and slope arrangement on pile group response in laterally spreading soils. J Geotech Geoenviron Eng. https://doi.org/10.1061/(ASCE)GT.1943-5606.0000654

Kramer SL (1996) Geotechnical earthquake engineering. Prentice Hall, Upper Saddle River, New Jersey, p 07458

Li G, Motamed R (2017) Finite element modeling of soil-pile response subjected to liquefaction induced lateral spreading in a large-scale shake table experiment. Soil Dyn Earthq Eng 92:573–584. https://doi.org/10.1016/j.soildyn.2016.11.001

Liu C, Tang L, Ling X, Deng L, Su L, Zhang X (2017) Investigation of liquefaction-induced lateral load on pile group behind quay wall. Soil Dyn Earthq Eng 102:56–64. https://doi.org/10.1016/j.soildyn.2017.08.016

Mao W, Liu B, Rasouli R, Aoyama S, Towhata I (2019) Performance of piles with different configurations subjected to slope deformation induced by seismic liquefaction. Eng Geol 263:105355. https://doi.org/10.1016/j.enggeo.2019.105355

Motamed R, Towhata I (2010) Shaking table model tests on pile groups behind quay walls subjected to lateral spreading. J Geotech Geoenviron Eng 136(3):477–489. https://doi.org/10.1061/(ASCE)GT.1943-5606.0000115

Motamed R, Towhata I, Honda T, Yasuda S, Tabata K, Nakazawa H (2009) Behaviour of pile group behind a sheet pile quay wall subjected to liquefaction-induced large ground deformation observed in shaking test in E-defense project. Soils Found 49(3):459–475. https://doi.org/10.3208/sandf.49.459

Motamed R, Sesov V, Towhata I, Anh NT (2010) Experimental modeling of large pile groups in sloping ground subjected to liquefaction-induced lateral flow: 1g shaking table tests. Soils Found 50(2):261–279. https://doi.org/10.3208/sandf.50.261

Motamed R, Towhata I, Honda T, Tabata K, Abe A (2013) Pile group response to liquefaction-induced lateral spreading: E-defense large shake table test. Soil Dyn Earthq Eng 51:35–46. https://doi.org/10.1016/j.soildyn.2013.04.007

Motamed R, Sesov V, Towhata I (2007) Study on P-Y curve for piles subjected to lateral flow of liquefied ground. In: Proceeding of The 14th world conference on earthquake engineering. Greece

Motamed R, Sesov V, Towhata I (2008) shaking model tests on behavior of group piles undergoing lateral flow of liquefied subsoil. In: Proceeding of the 4th international conference on earthquake geotechnical engineering. Beijing, China

Sato M, Tabata K (2011) Lateral spreading damage to sheet-pile walls and pile foundations reproduced by tsukuba large-scale shake table. J Earthq Tsunami 5(3):231–240. https://doi.org/10.1142/S1793431111001078

Su L, Tang L, Ling X, Liu C, Zhang X (2016) Pile response to liquefaction-induced lateral spreading: a shake-table investigation. Soil Dyn Earthq Eng 82:196–204. https://doi.org/10.1016/j.soildyn.2015.12.013

Suzuki H, Tokimatsu K, Sato M, Abe A (2006) Factor affecting horizontal subgrade reaction of piles during soil liquefaction and lateral spreading. Workshop on seismic performance and simulation of pile foundations in liquefied and laterally spreading ground. University of California, Davis, California, United States

Tamura K (2014) Seismic design of highway bridge foundations with the effects of liquefaction since the 1995 Kobe earthquake. Soils Found 54(4):874–882. https://doi.org/10.1016/j.sandf.2014.06.017

Tang L, Zhang X, Ling X, Su L, Liu C (2014) Response of a pile group behind quay wall to liquefaction-induced lateral spreading: a shake-table investigation. Earthq Eng Eng Vib 13(4):741–749. https://doi.org/10.1007/s11803-014-0263-8

Tang L, Ling X, Zhang X, Su L, Liu C, Li H (2015) Response of a RC pile behind quay wall to liquefaction-induced lateral spreading: a shake-table investigation. Soil Dyn Earthq Eng 76:69–79. https://doi.org/10.1016/j.soildyn.2014.12.015

Towhata L (2008) Geotechnical earthquake engineering. Springer

UCDavis, Civil and Environmental Engineering. https://research.engineering.ucdavis.edu/gpa/earthquake-hazards/liquefaction-ports.

Uzuoka R, Cubrinovski M, Sugita H, Sato M, Tokimatsu K, Sento N, Kazama M, Zhang F, Yashima A, Oka F (2008) Prediction of pile response to lateral spreading by 3-D soil-water coupled dynamic analysis: shaking in the direction perpendicular to ground flow. Soil Dyn Earthq Eng 28:436–452. https://doi.org/10.1016/j.soildyn.2007.08.007

Wang R, Fu P, Zhang JM (2016) Finite element model for piles in liquefiable ground. Comput Geotech 72:1–14. https://doi.org/10.1016/j.compgeo.2015.10.009

Zhang S, Wei Y, Cheng X, Chen T, Zhang X, Li Z (2020) Centrifuge modeling of batter pile foundations in laterally spreading soil. Soil Dyn Earthq Eng. 135:106166. https://doi.org/10.1016/j.soildyn.2020.106166

Zhu W, Gu L, Mei S, Nagasaki K, Chino N, Zhang F (2021) 1g model tests of piled-raft foundation subjected to high-frequency vertical vibration loads. Soil Dyn Earthq Eng. 141:106486. https://doi.org/10.1016/j.soildyn.2020.106486

Publisher's Note   Springer Nature remains neutral with regard to jurisdictional claims in published maps and institutional affiliations.